Payri, F.; Novella Rosa, R.; Pastor Enguídanos, JM.; Pérez-Sánchez, EJ. (2017). Evaluation of the approximated diffusion flamelet concept using fuels with different chemical complexity. Applied Mathematical Modelling. 49:354-374. doi:10.1016/j.apm.2017.04.024

Title:

Evaluation of the approximated diffusion flamelet concept using fuels with different chemical complexity

Authors:

F. Payri, R. Novella, J.M. Pastor and E.J. Pérez-Sánchez*

CMT-Motores Térmicos
Universitat Politècnica de València
Camino de Vera s/n, 46022,
Valencia (Spain)
Tel. (0034) 96 387 76 50 / Fax (0034) 96 387 76 59

Abstract

The ability of flamelet models to reproduce turbulent combustion in devices such as diesel engines or gas turbines has enhanced the usage of these approaches in Computational Fluid Dynamics (CFD) simulations. The models based on turbulent look-up tables generated from counterflow laminar diffusion flames (DF model) permit drastic reduction of the computational cost of the CFD calculation. Nevertheless, for complex molecular fuels, such as n-heptane, the oxidation process involves hundreds of species and the calculation of the transport equations together with the ODE system that models the chemical kinetics for the DF solution becomes unaffordable for industrial devices where hundreds of flamelets are required. In this context, new hypotheses have to be introduced in order to reduce the computational cost maintaining the coherence of the combustion process. Recently, a new model known as Approximated Diffusion Flamelet (ADF) has been proposed with the aim of solving the turbulent combustion for complex fuels in a reduced time. However, the validity of this model is still an open question and has to be verified in order to justify subsequent CFD calculations. This work assesses the ADF model and its ability to reproduce accurately the combustion process and its main parameters for three fuels with different chemical complexity and boundary conditions by its comparison with the DF model. Results show that although some discrepancies arise, the ADF model has the ability to correctly describe the ignition delay and the combustion structure in the auto-ignition zone that is the most relevant one for industrial processes.

Keywords:

Combustion modeling, Steady flamelet, Transient flamelet, Chemical kinetics, Tabulated chemistry

* *Corresponding author*
Email: edpresnc@mot.upv.es
Phone: (0034) 96 387 76 50 // Fax: (0034) 96 387 76 59

1. Introduction

During recent decades, the development of industrial combustion systems in terms of efficiency and pollutant emissions has encouraged the analysis of these systems by means of numerical simulations. In this context, the Computational Fluid Dynamics (CFD) is a powerful technique that allows the researcher to obtain very valuable knowledge of the turbulent combustion. Nevertheless, the models used for turbulent combustion are based on a set of hypotheses whose suitability depends on the combustion regime [1][2]. Together with the model hypotheses, the computational cost is another important factor that determines the model capabilities for practical applications.

Among the different models that can be found in the literature, the flamelet model is reported to be one of the most powerful models for solving the turbulent combustion [3][4]. For non-premixed turbulent combustion, the key underlying assumption of this model consists of describing the local structure of the turbulent flame by an ensemble of igniting and extinguishing laminar diffusion flames called flamelets. Thus, this assumption requires the chemistry to be much faster than physical processes such as the mixing process, corresponding to large Damköhler numbers. However, despite seeming very restrictive, this is usually a suitable description for non-premixed turbulent combustion in industrial devices and means that combustion takes place in a very thin layer in which the flamelets are embedded [2].

For non-premixed combustion systems, these flamelets usually follow a counterflow diffusion flame (DF) configuration. With the proper mathematical operations and simplifications, the flamelet can be described by a simplified 1D structure in the mixture fraction space [5]. The transport equations for temperature and species describing the flamelet evolution retain the transient, mixing and source terms. Mixing terms include the scalar dissipation rate (χ), which controls the diffusion rate of species in the mixture fraction space and depends on the strain rate (a) imposed by the flow [2] . Source terms for species transport equations are particularly critical since they are calculated by solving the stiff non-linear ODE system that models the chemical kinetics for each mixture fraction at each time

step. As the fuel increases in molecular complexity, its oxidation involves hundreds or even thousands of species and reactions. Therefore, the number of transport equations to be solved and the number of equations of the ODE system that models the chemical kinetics accordingly increase.

In recent decades, the flamelet model has been implemented following different approaches and it has been extensively applied especially in the field of the design and analysis of internal combustion engines.

In the representative interactive flamelet (RIF) model approach and its variants, the flamelet or set of flamelets required to reproduce the characteristics of the turbulent combustion is solved during the CFD computation [6][7]. However, despite the interesting results reported using this model, for instance in the field of diesel engines [8], this interactive coupling presents some important drawbacks related to the computational cost, i.e. the on-the-fly resolution of the set of flamelets, especially for fuels with high molecular complexity. In those cases, only a few flamelets are considered and the modeling of the turbulence-chemistry interaction (TCI) is partially lost [9].

In the approaches known as Flame Prolongation of Intrinsic Low-Dimensional Manifold (FPI), Flamelet Generated Manifold (FGM) and their respective variants, the set of flamelets required to reproduce the characteristics of the turbulent combustion is pre-calculated and, consequently, decoupled from the CFD computation. Results are stored in a look-up database in terms of thermochemical parameters [10][11][12]. These models are gaining attention since once the database is generated, the time required by the CFD computation for solving a given turbulent combustion problem is very limited. However, for fuels with high molecular complexity, the generation of the flamelet database is still too expensive in terms of computational cost and sometimes becomes unaffordable when the boundary conditions span over wide ranges of values and, consequently, a great number of flamelets have to be computed.

Recently, the Approximated Diffusion Flamelet (ADF) concept was developed with the aim of decreasing the computational effort required to generate the flamelet database while keeping complex chemistry [13]. The ADF concept is based on solving only the 1D flamelet transport equation for the progress variable, which is a linear combination of selected species that accounts for the transient evolution of the flamelet, in the mixture fraction space. Additionally, it decouples the mixing

and the source terms of this transport equation. The chemical source term of the progress variable is pre-calculated by solving the corresponding ODE system related to the chemical kinetics. For this purpose, the temporal evolution of a set of homogeneous reactors (HRs) for different mixture fractions is solved storing the results in a look-up table used when solving the progress variable transport equation [14]. It is important to note that since chemistry is decoupled from the diffusion processes the ADF model permits the modeling of complex chemistry in completely acceptable amounts of time.

The considerable reduction of calculation time gained with these simplifications allow the application of this flamelet model when the boundary conditions encompass a great variety of values, with flamelets belonging to the whole range of strain rates, while managing complex chemistry. These capabilities are particularly important in complex problems such as diesel engines where so many processes interact and the proper modelling of the phenomena is critical for describing the turbulent structure of the flame as well as predicting pollutant emissions.

Finally, these required modeling capabilities argue for the use of comprehensive mechanisms instead of reduced mechanisms that, certainly, would permit the application of the DF model but with losses that are not admissible for the previous modeling objectives.

In this context, the analysis of the flamelet steady-state conditions and their transient temporal evolution for both DF and ADF models are evaluated in the present investigation.

In a previous published study, the validity of the ADF assumptions was preliminarily investigated by directly comparing with the DF model keeping the same boundary conditions [13]. This analysis focused on evaluating the differences between DF and ADF related to the ignition delay, the initial ignition propagation across the flamelet and the steady-state reacting equilibrium conditions. In this research, despite the fact that noticeable discrepancies were clearly identified in all of the three characteristic flamelets investigated, the observed differences were considered acceptable. Nevertheless, the information reported was not sufficient to understand the extent of the differences between ADF and DF and/or how to decrease them since only very few flamelets (few strain rates) were considered [13]. The ADF concept was integrated into two similar flamelet combustion models, known as ADF-PCM (ADF Presumed Conditional Moment) and ADF-PCMχ

(ADF-PCM with probability density function in χ_{st}), and for both models the flamelet database was generated using this simplification.

These models have been applied during the last years to different problems such as lifted methane flames in a vitiated coflow [14], diesel-like sprays [15][16], diesel engines [17] and furnaces [18] and, in all cases, results were very promising. However, the validity of the ADF concept is still an open question nowadays under evaluation and more research effort is required.

In this framework, this investigation has the objective of evaluating in detail the ADF concept for reproducing the characteristics of the counterflow diffusion flamelets in the full range of strain rates until reaching the flamelet quenching conditions. Following the conventional approach, the analysis focuses on the key combustion characteristics including the ignition delay, the ignition propagation across the flame and the steady-state reacting equilibrium conditions. Additionally, the study also includes a dedicated discussion about the effect of the definition of the progress variable on the accuracy of the results provided by the ADF concept. Finally, three fuels (hydrogen, methane and n-heptane) are considered in this work in order to identify the impact of the fuel molecular complexity and to systematically analyze the validity of the ADF assumptions.

2. Description of the Diffusion Flamelets and Approximated Diffusion Flamelets

The scope of the present work only includes diffusion flamelets in an axisymmetric opposed-jet configuration. Assuming equal mass diffusion coefficients and heat capacities for all chemical species (constant with temperature) as well as unity Lewis number (equal thermal and mass diffusivities) the flamelet structure is completely defined by mixture fraction (Z) and time (t), so it can be described in the Z-space for each species by eq. (1) [2][19].

$$\frac{\partial Y_k}{\partial t} = \frac{\chi}{2}\frac{\partial^2 Y_k}{\partial Z^2} + \dot{\omega}_k \qquad k = 1, \ldots, N \tag{1}$$

where N is the total number of species of the chemical mechanism and Y_k is the

mass fraction of the species k. In eq. (1), $\chi = 2D|\nabla Z|^2$ is known as the scalar dissipation rate. This model considers a transient term ($\frac{\partial Y_k}{\partial t}$), a mixing term ($\frac{\chi}{2}\frac{\partial^2 Y_k}{\partial Z^2}$) and a chemical source term ($\dot{\omega}_k$). With the previous assumptions, the flamelet equation can be written in terms of temperature or mass fractions keeping exactly the same mathematical structure [5].

The steady flamelet equation is obtained by removing the transient term in eq. (1) and it is the basis of the Steady Flamelet Model (SFM), while retaining this transient term is the basis of the Unsteady Flamelet Model (UFM) [2].

The SFM model was used for a long time and is still valid when the chemical time scales are much smaller than the physical time scales (diffusion and convection) so Damköhler number tends to infinity and local equilibrium can be assumed [20]. This model provides the advantage of greatly simplifying the complexity of the problem, especially that related with chemistry modeling [21]. Nevertheless, it cannot reproduce the chemical impact of some species that are not in equilibrium, such as CO or NO_x, and the local quenching/ignition is not properly described. Therefore, this model is not appropriate for those problems where auto-ignition or local quenching/ignition are critical, such as the lifted flames [10][22].

These shortcomings can be mitigated by including the transient effects in the computations, i.e. UFM approach, for a more accurate description of the relevant phenomena involved in combustion. However, the better description of the processes is accompanied by a significantly higher computational cost, especially when dealing with fuels of complex chemistry. This justifies considering additional assumptions for the flamelet equation leading to the Approximated Diffusion Flamelet (ADF) model. This ADF model will be compared to the conventional Diffusion Flamelet (DF) model in the present work. In the following a description of the models used for this paper is given.

The DF model solves the flamelet equation in the Z-space, eq. (1), for each species accounted by the chemical kinetics mechanism. The steady-state scalar dissipation rate profile for laminar counterflow diffusion flames in the Z coordinate, given by eq. (2), is assumed [2]

$$\chi\,(a,Z) = \frac{a}{\pi}\exp[-2(erfc^{-1}(2Z))^2] \qquad (2)$$

In eq. (2), a is the strain rate and only depends on the flow characteristics.

Due to unity Lewis number, the total enthalpy is approximated as $h(Z) = Z \cdot h_f + (1 - Z) \cdot h_{ox}$, where h_f corresponds to the fuel enthalpy and h_{ox} to the oxidizer enthalpy. Then, the temperature is obtained from the total enthalpy and the chemical composition. In order to obtain the reaction rates for the species, a chemical balance considering the mechanism reactions for each species is solved at each time step. In this work, eq. (1) is solved in its steady and unsteady forms by means of the DDASSL solver [23], as in previous works [24]. Attending to the characteristics of the problem, a fine grid in the mixture fraction direction is defined in order to reduce numerical uncertainties especially at low strain rate values. The solutions for the DF model are obtained using LFLAM code developed at CIEMAT.

For the final tabulation of the transient thermochemical path followed by each mixture fraction, a variable that uniquely defines each state is required. For this purpose a progress variable Y_c, understood as a linear combination of species mass fractions, is used. This one-to-one relationship between time and Y_c (together with the continuity of Y_c) implies that Y_c is monotonous with time. Conventionally, Y_c is chosen increasing with time.

The ADF model also solves the flamelet equation in the Z-space, eq. (1), but only for the progress variable. As in the DF model, the steady-state profile for the scalar dissipation rate shown in eq. (2) is assumed. In order to simplify the chemical source term, it is not computed at each time step as in the DF model, but it is pre-calculated by solving the auto-ignition of a set of homogeneous reactors for each mixture fraction before the flamelet calculation is carried out. Thus, for each mixture fraction, the reaction rate of the progress variable is determined once the value of the progress variable is known independently of the strain rate. The flamelet equation can be rewritten as eq. (3) [13]

$$\frac{\partial Y_c}{\partial t} = \frac{\chi(a,Z)}{2}\frac{\partial^2 Y_c}{\partial Z^2} + \dot{\omega}_Y^{HR}(Z,c) \tag{3}$$

The dependences of the terms with the corresponding variables have been explicitly introduced in eq. (3) where c is the normalized progress variable. The independence of the reaction rate from the strain rate (no diffusion in homogenous reactors) points out that some diffusion contributions may not be reproduced by the model insofar as the chemical source term may be affected by these. The same progress variable solved in eq. (3) is also used for the final tabulation of the transient thermochemical path followed by each mixture fraction. By virtue of the

monotonically increasing relationship between time and Y_c it is deduced that $\dot{\omega}_Y^{HR}(Z, Y_c) \geq 0$.

The definition of the progress variable is a crucial step because, in any tabulated flamelet model that considers transient evolutions, the information retained depends on the relationship of the progress variable with the chemical evolution. Consequently, if for example, the progress variable does not change during an interval of the chemical process the chemical information is partially lost. In the case of the ADF model, the progress variable definition is even more critical because the capabilities of the model rely on its dependence with the chemical evolution from the very beginning.

To avoid these losses, it is advisable that the progress variable definition includes species related to the low and high temperature chemistry even though excellent results can be achieved if only intermediate species, such as CO, and final products, such as CO_2, are considered, as will be shown in this work.

For solving the ADF model, first, the HRs should be calculated and, in this work, this is carried out using the commercial software Chemkin [25]. For each mixture fraction the auto-ignition of a HR is solved with no heat losses and constant pressure as boundary conditions. The initial conditions are obtained from the adiabatic curve that is calculated from the composition and the temperature of the oxidizer and fuel streams. For avoiding uncertainties related to the discretization, the HRs transient evolutions are saved in increments of temperature equal or less than 0.5 K. Subsequently, the variables used in following calculations are stored in a table with the mixture fraction and the progress variable as inputs. For simplicity, the mixture fraction and the progress variable (normalized to chemical equilibrium) discretizations define a regular mesh.

For solving the steady regime of eq. (3) a Newton-Raphson algorithm is used. The profile for another strain rate, in general close to the one that is desired to solve, is provided as the initial solution for iteration. As the left hand side of eq. (3) vanishes for the steady calculation the following convergence criterion is imposed

$$abs\left(\frac{\chi(a,Z)}{2}\frac{\partial^2 Y_c}{\partial Z^2} + \dot{\omega}_Y^{HR}(Z, Y_c)\right) < 10^{-6} \qquad \forall Z \tag{4}$$

where abs is the absolute value and its argument corresponds to the right hand side of eq. (3). For the derivative, a second order discretization is used and the chemical

source term is obtained with a linear interpolation.

Finally, eq. (3) (transient regime) is solved for each strain rate using an implicit numerical scheme with adaptive time step and second order in mixture fraction and first order in time derivatives. As for the steady state calculation, a linear interpolation is used for retrieving the chemical source term. In order to minimize the impact of numerical uncertainties a fine mesh in mixture fraction and progress variable directions is chosen, as for the DF model. The rest of variables (temperature and species) are determined from the tables, also calculated from the auto-ignition of the corresponding HR, by means of linear interpolations. Note that the solutions for the temperature and the mass fractions of the species (except the progress variable) can be obtained during the post-processing and, therefore, reduce the computational time.

In Figure 1 and Figure 2, flowcharts show the steps required for solving both models.

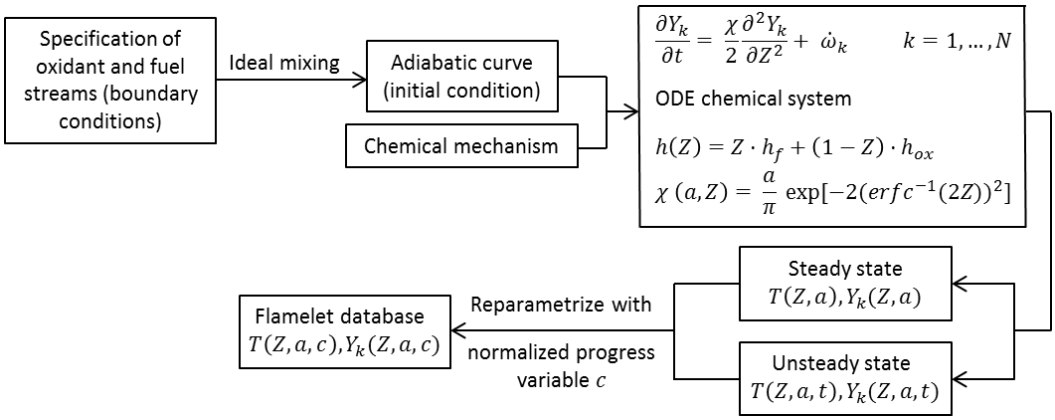

Figure 1. Flowchart for solving the DF model.

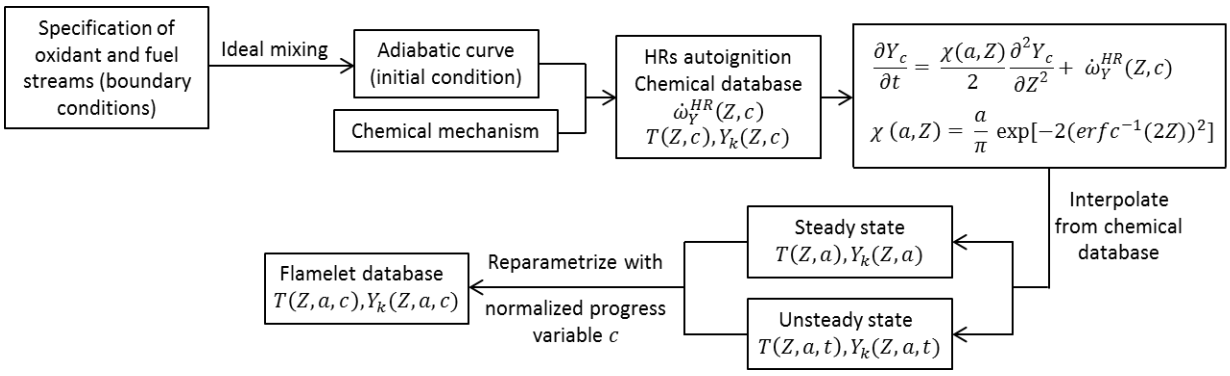

Figure 2. Flowchart for solving the ADF model.

Comparing DF and ADF models, it should be noticed how in the DF model the progress variable is only used for the final tabulation of the variables but not for computations as in the ADF model. Additionally, both models give the same solution when there is no diffusion in Z-space ($a = 0$) since the mixing term in eq. (1) and eq. (3) vanishes. The identical behavior of both models when $a \to 0$ explains why the chemical source terms and the rest of variables are retrieved from the HRs solution database for the ADF model, that is, that the DF model in the limit of low strain rates behaves as a set of HRs.

3. Methodology

The aim of this work is to determine the extent of applicability of the ADF model. To achieve this objective, a systematic analysis has been carried out which consists of the comparison of the steady and unsteady solutions between DF and ADF models for three fuels which comprise a range of hydrocarbon chemical complexity, namely hydrogen (H_2), methane (CH_4) and n-heptane (C_7H_{16}). Additionally, a study of the influence of the progress variable definition in the ADF results completes the work.

The specific boundary conditions for the set of flamelets resolved applying the DF and ADF methods for each fuel investigated are included in Table 1 (H_2), Table 2 (CH_4) and Table 3 (C_7H_{16}). With these conditions, the stoichiometric mixture fraction is 0.479 for H_2, 0.176 for CH_4 and 0.062 for C_7H_{16}. Additionally, the H_2 and the CH_4 flames develop in atmospheric conditions, so pressure equals 1 atm, whereas the pressure in the case of the C_7H_{16} flame is 42.1 bar.

Table 1. Boundary conditions for the H_2 set of flamelets.

	Fuel (Z = 1)	Hot coflow (Z = 0)
Temperature	305 K	1055 K
Mole fractions	$X_{H2,f} = 0.25$ $X_{N2,f} = 0.75$	$X_{O2,ox} = 0.1474$ $X_{N2,ox} = 0.7537$ $X_{H2O,ox} = 0.0989$

Table 2. Boundary conditions for the CH_4 set of flamelets.

	Fuel (Z = 1)	Hot coflow (Z = 0)
Temperature	320 K	1350 K

Mole fractions	$X_{O2,f} = 0.15$ $X_{N2,f} = 0.52$ $X_{CH4,f} = 0.33$	$X_{O2,ox} = 0.12$ $X_{N2,ox} = 0.73$ $X_{H2O,ox} = 0.15$

Table 3. Boundary conditions for the C_7H_{16} set of flamelets.

	Fuel (Z = 1)	Oxidant (Z = 0)
Temperature	373 K	1000 K
Mole fractions	$X_{C7H16} = 1$	$X_{O2,ox} = 0.21$ $X_{N2,ox} = 0.79$

These fuels and boundary conditions correspond to three experimental configurations, namely the lifted hydrogen and methane jet flames in a vitiated coflow from the University of Berkeley and the spray H from the ECN (Engine Combustion Network), for C_7H_{16} [26][27][28], extensively used for combustion validation.

For H_2 fuel, the chemical kinetics mechanism includes 9 species and 21 reactions [29]. For CH_4 the well-known GRI chemical kinetic mechanism was selected, which involves 53 species and 325 reactions [30]. Finally, for C_7H_{16} the chemical kinetics mechanism developed by Zeuch et al. considers a total of 110 species and 1170 forward and backward reactions [31].

Since fuels of different molecular complexity are chosen for comparing the DF and the ADF models, the analysis starts with the simplest fuel (H_2), follows with the simplest hydrocarbon (CH_4) and finally ends with a complex hydrocarbon (C_7H_{16}), which is usually used as a chemical surrogate for diesel fuels.

The definition of the progress variable for hydrogen is $Y_c = Y_{H2O} + 10\,Y_{HO2} + 3\,Y_{H2}$ which has been used by Naud et al. for the simulation of the aforementioned lifted hydrogen jet flame in a vitiated coflow experiment from the University of Berkeley [24]. For methane and n-heptane, two progress variables are considered. The first (PV1) is defined as $Y_c = Y_{CO} + Y_{CO2}$ [13] and the second (PV2) is defined as $Y_c = Y_{CO} + Y_{CO2} + Y_{H2O} + 10\,Y_{HO2} + 3\,Y_{H2}$ which is the sum of PV1 plus the progress variable used for hydrogen.

PV1 is a progress variable definition that has been often used for the SFM approaches and, lately, its use has been extended to USFM computations. It is

observed that this definition is based on an intermediate species, such as CO, and a final product, namely CO_2, of the combustion. Consequently, it is suitable for the tabulation of steady flamelets. Given that the transient evolution of the flamelets becomes essential when studying the auto-ignition and the pollutant emissions in turbulent reactive flows it is interesting to maintain an accurate description of the process of the unsteady ignition prior to the main combustion. For that purpose, intermediate species, such as HO_2, weighted with different coefficients are included in the PV2 definition. The sum of PV1 plus the progress variable $Y_c = Y_{H2O} + 10\,Y_{HO2} + 3\,Y_{H2}$, used for the simulation of hydrogen, is proposed as an alternative definition of the progress variable (PV2) for the methane and the n-heptane fuels.

It has been checked that these definitions for the progress variable provide in all cases a one-to-one relationship between them and time, fulfilling the main constraint imposed on a progress variable definition.

In principle, PV2 is used for CH_4 calculations while PV1 is used for C_7H_{16} unless otherwise indicated.

To determine the capabilities of the ADF model a fair comparison between DF and ADF models avoiding numerical uncertainties is considered a priority. For that purpose, fine grids have been selected in the mixture fraction and progress variable directions although for practical calculations, i.e. CFD computations, satisfactory results can be achieved using coarser meshes.

In the tabulation of the HRs 201 points equally spaced in the mixture fraction direction were selected for H_2 and 251 points for CH_4 while 338 points were chosen for C_7H_{16} with a distribution depending on the fuel equivalence ratio. The distribution in the (normalized) progress variable direction is common for all the fuels with 504 points equally spaced except for low values of the progress variable where the mesh is finer. In the case of the DF model, 201 points equally spaced in the mixture fraction direction were selected for the H_2 and 501 points for both CH_4 and C_7H_{16}. As a final remark, all flamelet calculations for both DF and ADF models were performed keeping the mixture fraction boundaries at their natural limits, 0 in the oxidizer side and 1 in the fuel side.

4. Results and discussion

The discussion of the results provided by the DF and ADF models is carried out sequentially and, therefore, as a first step, the analysis starts for the steady-state

regime, where the models are compared by observing the structure of the so-called S-curves. As a second step, the analysis is completed with the study of the unsteady (or transient) solutions, where the models are compared in terms of the ignition delay and ignition propagation across the flamelet.

Since the scalar dissipation rate (χ) is directly related to the strain rate (a), considering eq. (2), both parameters will be used to characterize the strength of the mixing in the flamelet.

Steady regime

After obtaining the steady-state solutions for the entire range of strain rates (or scalar dissipation rates) where the laminar combustion develops, it is possible to draw the tridimensional surface, in the variables (Z, χ, Y_c), containing all the possible states for the steady-state regime. One of the most important properties of these surfaces is that they define the physical limits of the unsteady solutions, which fill the inner space of the surface created by these steady-state solutions. Such surfaces are shown for the DF and ADF models and the three fuels in Figure 3. Each color is related to a different branch of the S-curve, as explained later. Scales are common for figures corresponding to the same fuel.

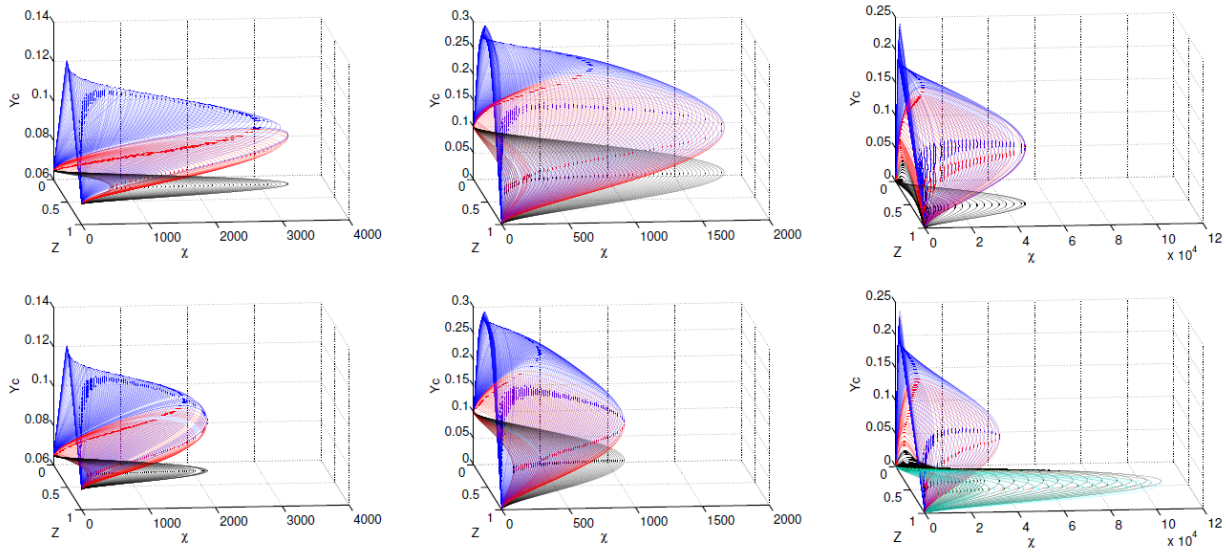

Figure 3. Steady-state flamelets solved with the DF (top) and ADF (bottom) models. Solutions for H_2 (left), CH_4 (center) and C_7H_{16} (right).

The most important qualitative divergences observed comparing DF and ADF solutions are related to the maximum χ attainable before reaching the quenching

conditions (χ_q), represented by the line joining the blue and the red surfaces. As a common trend independent of the fuel, χ_q is significantly higher for DF than for ADF and, consequently, the DF model sustains the combustion in more highly strained flows compared to the ADF model. Thus, considering that increasing flow turbulence reflects in higher local values of χ, the ADF model is expected to predict quenching at high flow turbulence levels where the DF model would predict that it is sustained.

A second difference observed in these steady-state solutions, though only for the C_7H_{16} case, is related to the second peak generated by the ADF model in the right side of the surfaces (at high χ and low Y_c values) joining the black and the green surfaces. The DF model does not generate this second quenching point and it seems to be unrealistic considering the physics of the problem. Note how in the case of C_7H_{16} it is around three times higher than the physical χ_q. Therefore, it seems that the chemical kinetics of the fuel has influence on the generation of this second quenching point as well as on its magnitude. A further detailed discussion on this topic is later exposed.

Once the DF and the ADF steady-state solutions have been compared, more quantitative information is obtained by observing the well-known S-curve for the progress variable. This S-curve is generated by cutting the surface of steady-state solutions at a given Z value. As is known the S-curve is composed of different branches which define the stability of the solution to small perturbations of the strain rate in the flame. Generally speaking, the S-curve is composed of three branches that are identified with an upper stable branch close to the chemical equilibrium (blue surface in Figure 3), an unstable branch at high strain rates and intermediate progress variable values (red surface in Figure 3) and a lower stable branch (black surface in Figure 3) that at high strain rates overlaps with the inert curve. However, as previously indicated, the n-heptane shows two unstable branches when solved with the ADF model.

The S-curves for three different values of Z corresponding to lean, stoichiometric and rich conditions are shown in Figure 4 (H_2), Figure 5 (CH_4) and Figure 6 (C_7H_{16}). For simplicity, the strain rate (a) is used to plot the S-curves instead of the scalar dissipation rate (χ).

Figure 4 corroborates how for H_2 the DF model gives a greater a value for the quenching point (a_q=10365 1/s) than the ADF (a_q=6550 1/s). The same

consideration is also valid for the maximum auto-igniting strain rate (a_{AI}), which is the strain rate that corresponds to the left side peak at low Y_c observed in the S-curve. This point is important since it corresponds to the highest value of a or χ, namely a_{AI} or χ_{AI}, at which the flamelet can evolve from the inert conditions until reaching the upper steady-state branch, and then, it limits what is known as the flamelet auto-ignition range. The rest of the domain corresponds to the ignition-extinction range.

Whereas in the DF model a_{AI} equals 2000 1/s, in the ADF model it only reaches 850 1/s. This means that the diffusion processes in Z-space affect the evolution of the chemical kinetics and these processes are not taken into account in the ADF model because the chemistry path comes from the auto-ignition of homogenous reactors. Note how in the auto-ignition range with strain rates below a_{AI}, differences in the S-curve are not as important as in the ignition-extinction range with strain rates over a_{AI}. This limits the validity of the ADF concept in the ignition-extinction range even for low molecular complexity fuels.

Figure 5 shows the corresponding S-curves for CH_4. Consistently, the DF model increases the quenching strain rate (a_q=5550 1/s) compared to the ADF model (a_q=3200 1/s). However, contrary to results with H_2, in this case the maximum auto-ignition strain rate is lower for the DF model (a_{AI}=360 1/s) than for the ADF model (a_{AI}=570 1/s). Results corroborate the key two ideas extracted from the H_2 analysis, namely the validity of the ADF assumptions in the auto-ignition range and the discrepancies observed in the ignition-extinction range.

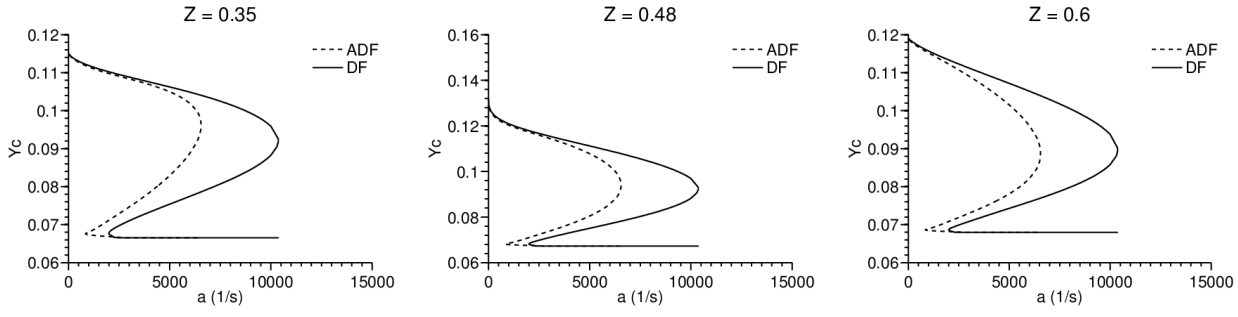

Figure 4. S-curves obtained for H_2 with the DF and ADF models for lean (left), stoichiometric (center) and rich (right) mixtures.

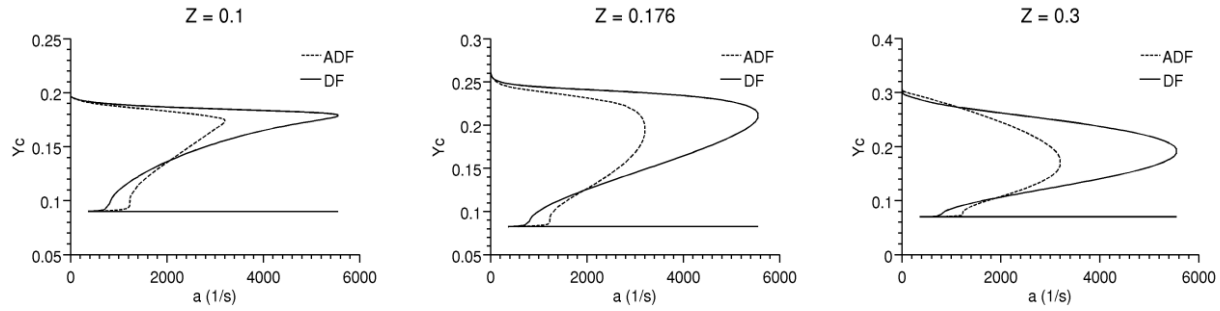

Figure 5. S-curves for CH_4 obtained with the DF and ADF models for lean (left), stoichiometric (center) and rich (right) mixtures.

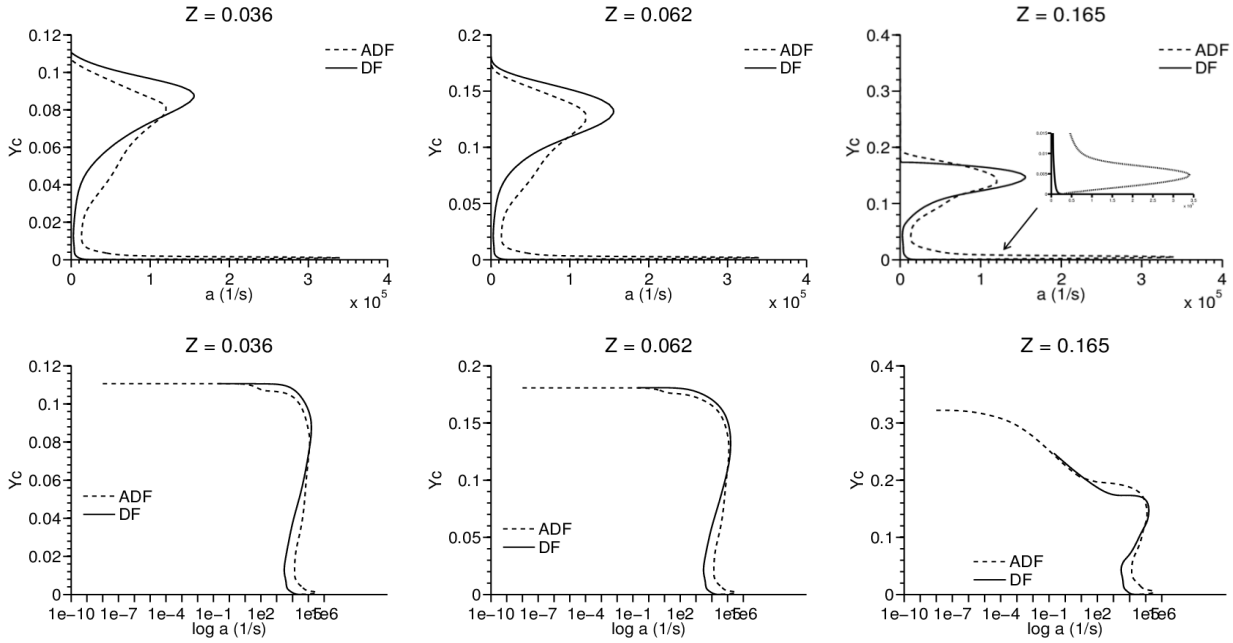

Figure 6. S-curves for C_7H_{16} in linear (top) and logarithmic (bottom) x-axis obtained with the DF and ADF models for lean (left), stoichiometric (center) and rich (right) mixtures.

To close the analysis of the steady-state conditions, Figure 6 shows the S-curves for C_7H_{16}. Due to the wide range of strain rates, figures have been represented using linear and logarithmic scales on the abscissa axis. As observed in Figure 6, the solutions for DF and ADF are close in the auto-ignition range (clearly seen in figures with logarithmic scales). Nevertheless, as it was pointed out before, a second non-physical quenching point at low Y_c values, which is shown with a zoom in Figure 6 top right for better visibility, is observed in the ADF S-curves for this fuel. The physical quenching strain rate keeps the trend of being higher for the DF model (a_q=155550 1/s) than for the ADF model (a_q=120000 1/s). The maximum auto-ignition strain rate, a_{AI}, is lower for DF (a_{AI}=2990 1/s) than for ADF (a_{AI}=13400 1/s) showing the same trend than that observed for CH_4.

The geometry of the S-curves for the C_7H_{16}, with the two quenching points, is explained by looking at the contour plots included in Figure 7. These contour plots represent the chemical source terms given by the auto-ignition of the homogeneous reactors for each mixture fraction. The axes are the mixture fraction and the normalized progress variable defined by eq. (5), where $Y_{c,inert}$ and $Y_{c,equil}$ correspond to the inert and chemical equilibrium values of the progress variable.

$$c(Z,t) = \frac{Y_c(Z,t) - Y_{c,inert}(Z)}{Y_{c,equil}(Z) - Y_{c,inert}(Z)} \tag{5}$$

Due to the monotonic increasing evolution of the progress variable it is deduced that $c \in [0,1]$.

Only for C_7H_{16}, two maxima at relatively low and high values of c can be observed in the contour plot, directly related to the complexity of the ignition process of long chain alkanes, while H_2 and CH_4 only show one maximum at relatively high values of c. Considering eq. (3) and removing the transient term due to the steady-state regime condition, and having in mind that the whole set of steady solutions covers all the possible states between the inert and the equilibrium solutions, it is deduced that an increase of the chemical source term must be compensated by an increase (in absolute value) of the mixing term. This term is the product of the second derivative of Y_c with respect to Z and the diffusion coefficient represented by $\chi(a, Z)$. However, the increase of the chemical source term around the maxima is not fully compensated by the second derivative, forcing the increment of $\chi(a, Z)$, and particularly of a. This generates the two quenching points in the S-curves clearly observed for the C_7H_{16} fuel in Figure 6.

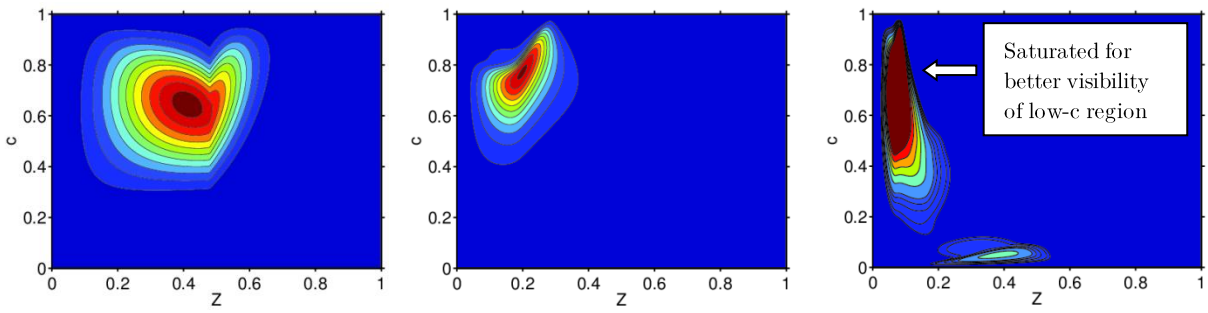

Figure 7. Chemical source terms obtained from the HRs for H_2 (left), CH_4 (center) and C_7H_{16} (right).

This behavior can be clearly observed in Figure 8 where some steady solutions (Z, Y_c) obtained with the ADF model are plotted together with different level curves corresponding to the chemical source term $\dot{\omega}_Y^{HR}$ for the n-heptane. It is evident that the change of branch takes place in the vicinity of a local maximum/minimum of the chemical source term. The low values that the term $\partial^2 Y_c / \partial Z^2$ takes (if this term is identified in a first approximation with the curvature it is seen that the curvature is very low for some curves as those drawn in red) imply that the chemical term has to be compensated with the strain rate value, that appears in the mixing term, generating the different branches of the S-curve. In general, the number of local maxima of the chemical field $\dot{\omega}_Y^{HR}(Z, Y_c)$ coincides with the number of pairs of stable-unstable branches of the S-curve.

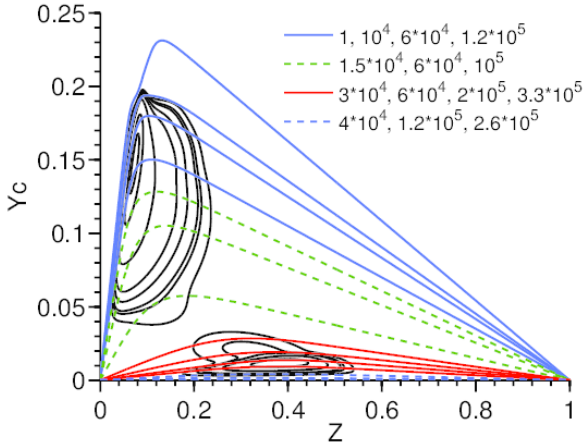

Figure 8. Steady solutions (Z, Yc) for the ADF model superimposed on the level curves of the chemical source field (black lines) for the C_7H_{16}. Each type of line corresponds to a different branch of the S-curve. The values of the legend indicate the strain rate (1/s) values of the solutions plotted.

In conclusion, although C_7H_{16} is the fuel with the most complex chemistry of those under investigation, even in this case, the ADF model assumptions are still valid in the auto-ignition range. However, considering the set of three fuels, it is observed that the ADF assumptions are less acceptable in the ignition-extinction range independent of the chemical complexity of the fuel.

Effect of the progress variable definition

In the ADF model the definition of Y_c has intrinsic impact on the results because this parameter is the tracer of the combustion process and thus, only the chemical kinetics information retained by Y_c can be retrieved later. It is evident that in the DF model the choice of Y_c cannot affect the results because all the species are solved and Y_c is calculated during the post-processing.

Thus, in order to determine the impact of the definition of Y_c, two definitions, PV1 and PV2, described in the Methodology section are used for comparing the S-curves of the ADF steady-state solutions for CH_4 and for C_7H_{16} in Figure 9 and Figure 10, respectively. Again for Figure 10 linear and logarithmic scales are used on the abscissa due to the broad range of a. Because of the different definition of Y_c they cannot be compared directly and so, to overcome this problem, the comparison is carried out using the temperature instead of the progress variables.

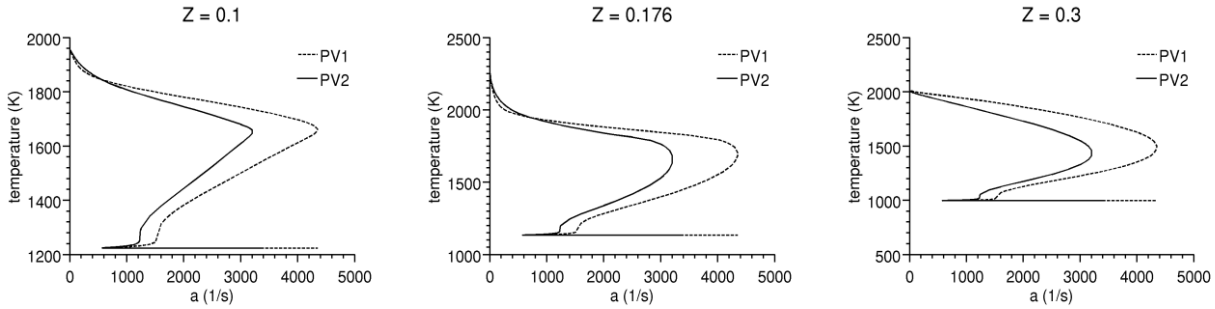

Figure 9. S-curves for CH_4 obtained with the ADF model using PV1 and PV2 for lean (left), stoichiometric (center) and rich (right) mixtures.

Expected differences are confirmed by the results and, although both Y_c definitions present relevant differences in the ignition-extinction range the auto-ignition range is similarly reproduced. Additionally, for a given a value these differences are more evident for rich mixture fractions than for stoichiometric or lean conditions.

In Figure 10, two quenching points appear in the S-curve for C_7H_{16} with both Y_c definitions. The main difference between the curves is found in the region close to the second low peak (high a and low Y_c). Excepting this zone, the rest of the curve is similarly reproduced by PV1 and PV2.

Thus, for fuels like CH_4 the S-curves obtained with ADF can be reasonably adjusted to those obtained with DF by a proper Y_c definition. However, for long chain alkane fuels like C_7H_{16} the second non-physical quenching point (at low Y_c values) can be decreased but not fully avoided since, as discussed previously using Figure 7 and Figure 8, it basically depends on the ignition chemical characteristics of the fuel.

In conclusion, it can be stated that although non-negligible discrepancies arise in the ignition-extinction range, the auto-ignition range is correctly described and, therefore, differences are acceptable in this range. This is an important conclusion because in a great number of industrial applications, such as diesel engines, the turbulent combustion develops in a turbulent flow basically matching the auto-

ignition range (lower strain rates than a_{AI}) and the ignition-extinction range is much less relevant, and most times negligible. Thus, in the field of diesel engine combustion modeling, good results have been reported in the literature using the ADF model only in the auto-ignition range, sustaining the assumption that it is mostly the range affecting the problem and validating the ADF model [16][17].

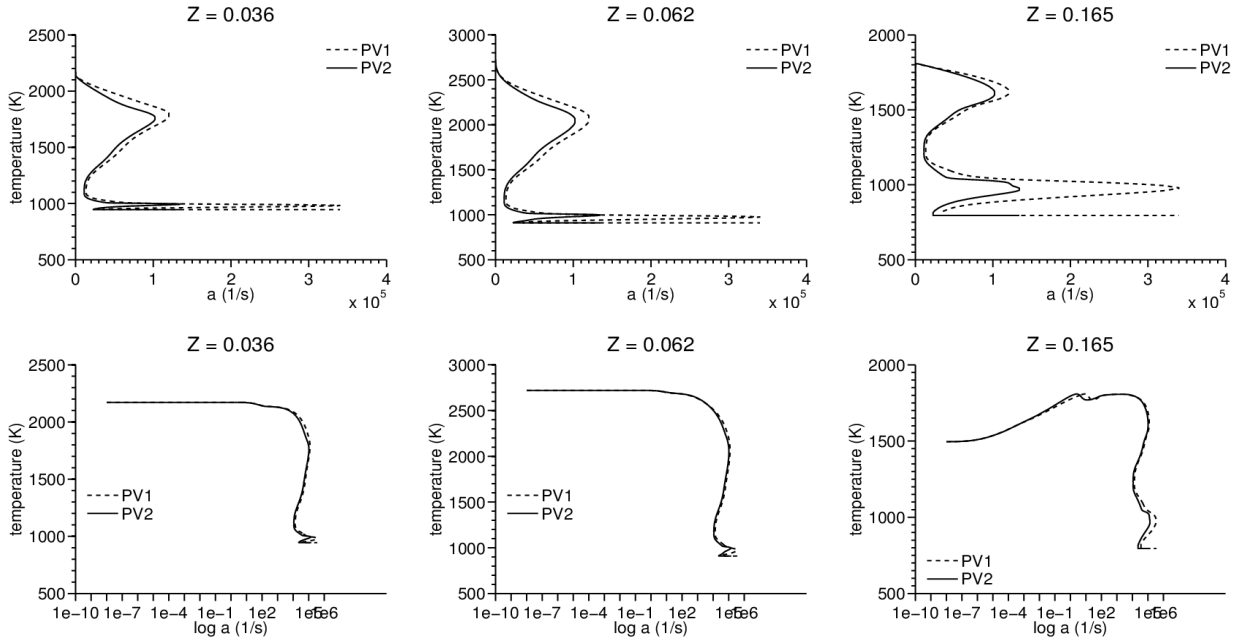

Figure 10. S-curves for C_7H_{16} in linear (top) and logarithmic (bottom) x-axis using PV1 and PV2 for lean (left), stoichiometric (center) and rich (right) mixtures.

Unsteady regime

In this section DF and ADF models will be compared in unsteady conditions for H_2, CH_4 and C_7H_{16}. First, a comparison of the computational cost for transient calculations between both models is carried out. Later, a discussion about fitting the first tabulated values of the chemical source term required for recovering the auto-ignition of the HRs when reconstructed is presented. The section continues with the comparison of the ignition delays and the structure combustion given by both models. Finally, a discussion of the effect of the progress variable definition is included.

Comparison of the computational cost

In this subsection, a comparison of the time spent for solving flamelets at different strain rates for both models is provided. Only results for n-heptane are included since it is the most representative fuel of those examined in this work having in mind that the ADF model is conceived for being used when complex chemistry is

mandatory. In the case of the C_7H_{16}, the time spent for solving a given flamelet with the DF model is in the order of tens of minutes, nevertheless, the ADF model allows the computational cost calculation for a flamelet to be decreased to a few minutes. Table 4 gathers the computational time required for solving several flamelets with different strain rate values for both models and the time spent for calculating the HRs database.

Table 4. Comparison of the computational time for DF and ADF models for C_7H_{16}. Strain rate units in 1/s. Computational time units in minutes. Machine characteristics: RAM memory of 64 GB, clock frequency of 2.5 GHz. All the calculations launched at one core.

	HRs	$a = 1$	$a = 10$	$a = 50$	$a = 100$	$a = 200$	$a = 1000$
DF	-	107	74	55	48	39	23
ADF	45	6	8	3	3	2	2

From Table 4 it is observed that the ADF model reduces the computational time required for each flamelet by at least one order of magnitude. Additionally, it is clear that the computational cost is reduced when increasing the strain rate.

Consequently, if a flamelet database is composed of 30 flamelets considering an average computational time per flamelet of 55 minutes for the DF model it takes 1650 minutes (=55*30). Nevertheless, using the ADF model and considering an average computational time per flamelet of 4 minutes and 45 minutes for the HRs calculation this time is reduced to 165 minutes (=45+4*30).

Thus, when considering complex problems such as the ignition in diesel engines, where due to the boundary conditions several hundreds or even thousands of flamelets are computed, the computational time required when using the DF model becomes prohibitive while using the ADF model is still feasible.

Discussion about the integration of the chemical source term

Before solving the transient flamelet equation, some considerations about the chemical source term may be established. It is known that in tabulated methods, such as the ADF model, a fine discretization in the progress variable direction is needed when taking the chemical source term directly from the chemical HRs database [32]. In this section, a method based on the linear interpolation of the chemical source term is discussed in order to obtain a good description of the

ignition delay and the auto-ignition of the HRs with coarser meshes in c.

A piecewise linear interpolation in the progress variable direction is used for all the variables, including the chemical source term, when retrieving the HRs information for the ADF calculations. In general terms, the first tabulated value for the chemical source term of the progress variable (that is $\dot{\omega}_{Y_0} = \dot{\omega}_Y(c = 0)$) is very low and small errors introduce artificial delays in the HR ignition when reconstructed. Consequently, it is important to calculate this first value accurately in order to retrieve the profile $Y_c = Y_c(t)$ given by the solution of the HR. Additionally, for avoiding numerical perturbations for the transient calculations it is recommendable that the chemical source term is described by a continuous function. For this purpose, the following method, that fulfills the previous requirements and gives excellent results in the reconstruction of the HRs from the tabulated chemical source terms, is presented.

Consider the solution of a HR for a given mixture fraction Z and let $\dot{\omega}_{Y_0} = \dot{\omega}_Y(c = 0)$, that is unknown, and $\dot{\omega}_{Y_1} = \dot{\omega}_Y(c = c_1)$ and $t_1 = t(c = c_1)$ the values obtained from the HR solution for the first non-null tabulated value of the c mesh, where c is normalized with the chemical equilibrium. For the moment, it is supposed that these values at $c = c_1$ are known. The aim is to obtain the value $\dot{\omega}_{Y_0}$ needed to reach a value c_1 in a time t_1 when the HR is reconstructed.

As a piecewise linear interpolation is used, the $\dot{\omega}_Y$ values for $c \in [0, c_1]$ can be written in the form $\dot{\omega}_Y = m * c + \dot{\omega}_{Y_0}$ where m is the slope of the straight line and its value is $\frac{\dot{\omega}_{Y_1} - \dot{\omega}_{Y_0}}{c_1}$. In this way, the following equation can be posed

$$\dot{\omega}_c = \frac{\dot{\omega}_Y}{Y_{c,equil} - Y_{c,inert}} = \frac{dc}{dt} \rightarrow \int_0^{t_1} \frac{dt}{Y_{c,equil} - Y_{c,inert}} = \int_0^{c_1} \frac{dc}{\dot{\omega}_Y} \tag{6}$$

and solving

$$\frac{t_1}{Y_{c,equil} - Y_{c,inert}} = \int_0^{c_1} \frac{dc}{m * c + \dot{\omega}_{Y_0}} = \frac{1}{m} ln\left(\frac{m * c_1 + \dot{\omega}_{Y_0}}{\dot{\omega}_{Y_0}}\right) = \frac{c_1}{\dot{\omega}_{Y_1} - \dot{\omega}_{Y_0}} ln\frac{\dot{\omega}_{Y_1}}{\dot{\omega}_{Y_0}} \tag{7}$$

which can be rewritten as (calling $\frac{t_1}{Y_{c,equil} - Y_{c,inert}}$ for simplicity as $t_1{}'$)

$$\frac{e^{\frac{t_1{}'}{c_1}\dot{\omega}_{Y_1}}}{\frac{t_1{}'}{c_1}\dot{\omega}_{Y_1}} = \frac{e^{\frac{t_1{}'}{c_1}\dot{\omega}_{Y_0}}}{\frac{t_1{}'}{c_1}\dot{\omega}_{Y_0}} \tag{8}$$

With the notation $A = \frac{e^{\frac{t_1'}{c_1}\dot{\omega}_{Y_1}}}{\dot{\omega}_{Y_1}}$ and $= \frac{t_1'}{c_1}$, eq. (8) takes the final form

$$-\frac{B}{A} = -B\dot{\omega}_{Y_0} e^{-B\dot{\omega}_{Y_0}} \tag{9}$$

This equation is of the form $M = ze^z$ where M is known (in eq. (9) it corresponds to $-B/A$) and z is unknown (in eq. (9) it corresponds to $-B\dot{\omega}_{Y_0}$). The solution to this equation is given by the inverse of the function $f(x) = xe^x$ which is called the Lambert W function and is shown in Figure 11. The W function is a multivalued function (except at 0). If $W(x)$ is restricted to real values it is defined for $-1/e \leq x$ and is composed of two branches (solutions), W_0 and W_{-1}. If $x \geq 0$ the only real value solution is given by the branch 0 (W_0). For $-1/e \leq x < 0$ the solutions are given by the branch 0, with $W_0 \geq -1$, and the branch -1 (W_{-1}), with $W_{-1} < -1$, as can be observed in Figure 11.

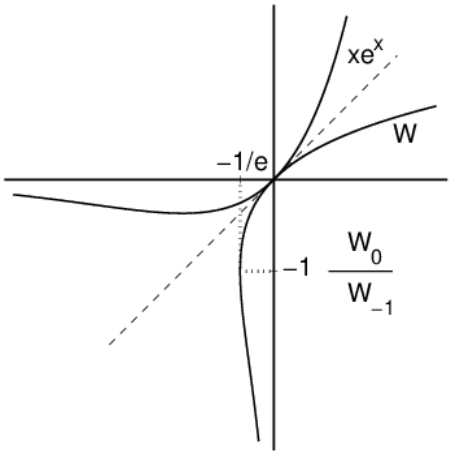

Figure 11. Function f(x)=xe^x and its inverse Lambert W function defined for real values. The two branches W_0 and W_{-1} are also indicated.

As $A, B > 0$ the left hand side of eq. (9) is negative and due to

$$-\frac{B}{A} = -\frac{t_1'}{c_1}\dot{\omega}_{Y_1} e^{-\frac{t_1'}{c_1}\dot{\omega}_{Y_1}} \in Im(xe^x) \rightarrow -\frac{B}{A} \geq -\frac{1}{e}$$

where Im is the image of the function. It is deduced that $-\frac{1}{e} \leq -\frac{B}{A} < 0$ so the problem has solution and is given by W_0 or by W_{-1}. Note that eq. (8) has two solutions, the trivial $\dot{\omega}_{Y_1}$ solution (replacing $\dot{\omega}_{Y_0}$ by $\dot{\omega}_{Y_1}$ in the right hand side it gives the identity) and the non-trivial $\dot{\omega}_{Y_0}$ solution. Therefore, the solutions to eq. (9) are $-B\dot{\omega}_{Y_1}$ and $-B\dot{\omega}_{Y_0}$ although only the solution $-B\dot{\omega}_{Y_0}$ is retained. (Note: $-B\dot{\omega}_{Y_1}$ is not a valid solution to the problem because in eq. (7) it is implicitly supposed $m \neq 0$.)

In this way, the solutions $-B\dot{\omega}_{Y_1}$ and $-B\dot{\omega}_{Y_0}$ are given one by W_0 and the other one by W_{-1}. Considering that $W_0 \geq -1$ and $W_{-1} < -1$, it can be established that if $-B\dot{\omega}_{Y_1} \geq -1$ the trivial $-B\dot{\omega}_{Y_1}$ solution is given by W_0 and so $-B\dot{\omega}_{Y_0}$ is defined by W_{-1} and vice versa. So, finally, the solution is

$$\dot{\omega}_{Y_0} = \begin{cases} -\dfrac{W_0(-\frac{B}{A})}{B} & if -B\dot{\omega}_{Y_1} < -1 \\ -\dfrac{W_{-1}(-\frac{B}{A})}{B} & if -B\dot{\omega}_{Y_1} \geq -1 \end{cases} \tag{10}$$

In the case that the values t_1 and $\dot{\omega}_{Y_1}$ for c_1 are unknown (not enough resolution) the same reasoning can be applied to the first c tabulated value with available information and $\dot{\omega}_Y$ is linearly interpolated for the c tabulated values between $c = 0$ and this first c tabulated value with information.

Finally, note that with a piecewise linear interpolation for $\dot{\omega}_Y = \dot{\omega}_Y(c)$ the reconstructed profile $c = c(t)$ for the HR correspond to piecewise exponential curves (as it is observed writing eq. (7) as a function $c = c(t)$) which provide a very close curve to the solution $c = c(t)$ provided by the HR tabulated solution, especially before the auto-ignition.

In conclusion, if the first value of the chemical source term is adjusted with this method it is not necessary to use a very fine discretization at low c values and the reconstructed ignition profile is very close to the real evolution of the HRs. Additionally, as was pointed out before, the use of a piecewise linear profile allows modeling the chemical source term with a continuous function, which is useful for further calculations.

Ignition delay and combustion structure

The study of the unsteady regime starts by the analysis of the ignition delay curves. The ignition delay curve for a given auto-igniting flamelet is obtained from the time spent by each mixture fraction to reach a predefined value of the normalized progress variable, c_F, calculated according to eq. (11):

$$c_F(Z, a, t) = \frac{Y_c(Z, a, t) - Y_{c,inert}(Z)}{Y_{c,steady}(Z, a) - Y_{c,inert}(Z)} \tag{11}$$

where $Y_{c,inert}(Z)$ and $Y_{c,steady}(Z, a)$ correspond to the inert and the steady values of

the progress variable, respectively.

As c_F measures the advancement of the flame referred to its steady state, in this work, two values of c_F for measuring the ignition delay have been chosen, namely 0.05 and 0.3, corresponding respectively to the very beginning of the combustion process and to a more developed stage [13][33]. In this way, the behavior for low-temperature and high-temperature chemistry, with a notable different evolution especially for long chain alkanes as n-heptane, is analyzed with these two values of c_F.

Thus, the ignition delay curves for the flamelets calculated with DF and ADF models at three different a values belonging to the auto-ignition range are included in Figure 12 for H_2 and in Figure 13 for CH_4. Scales are common for figures corresponding to the same strain rate value.

Results show how both DF and ADF models take into account diffusive processes in the Z-space since the ignition delay curves are sensitive to changes in the strain rate. For the two fuels, the shape of the curves provided by the DF and ADF models is similar, however the models progressively diverge as a increases. Hence, it is observed that the ADF model provides satisfactory results for all the cases shown in Figure 12 and Figure 13 except for the highest strain rate, that is, close to a_{AI}.

As previously explained, by definition both models give the same solution when there is no strain rate, $a = 0$, and the ignition-extinction zone is not well-reproduced by the ADF model. Consequently, it is expected that the divergence between models appears in a progressive way in the vicinity of a_{AI} as shown in the figures. Therefore, there should be an excellent agreement for low a values while for high a values, close to the a_{AI} limit, the ability of the ADF model to predict the ignition delay is compromised.

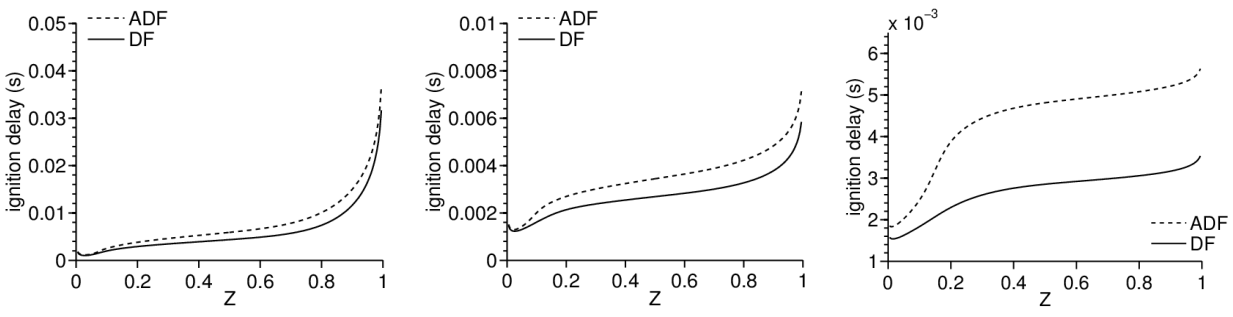

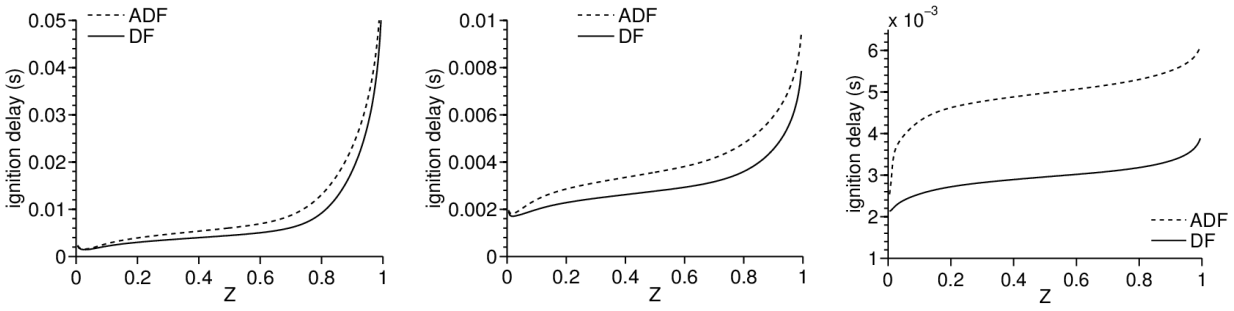

Figure 12. Ignition delay time for H_2 until reaching c_F=0.05 (top) and c_F=0.3 (bottom) at strain rates a=10 (left), a=100 (center) and a=600 (right) 1/s.

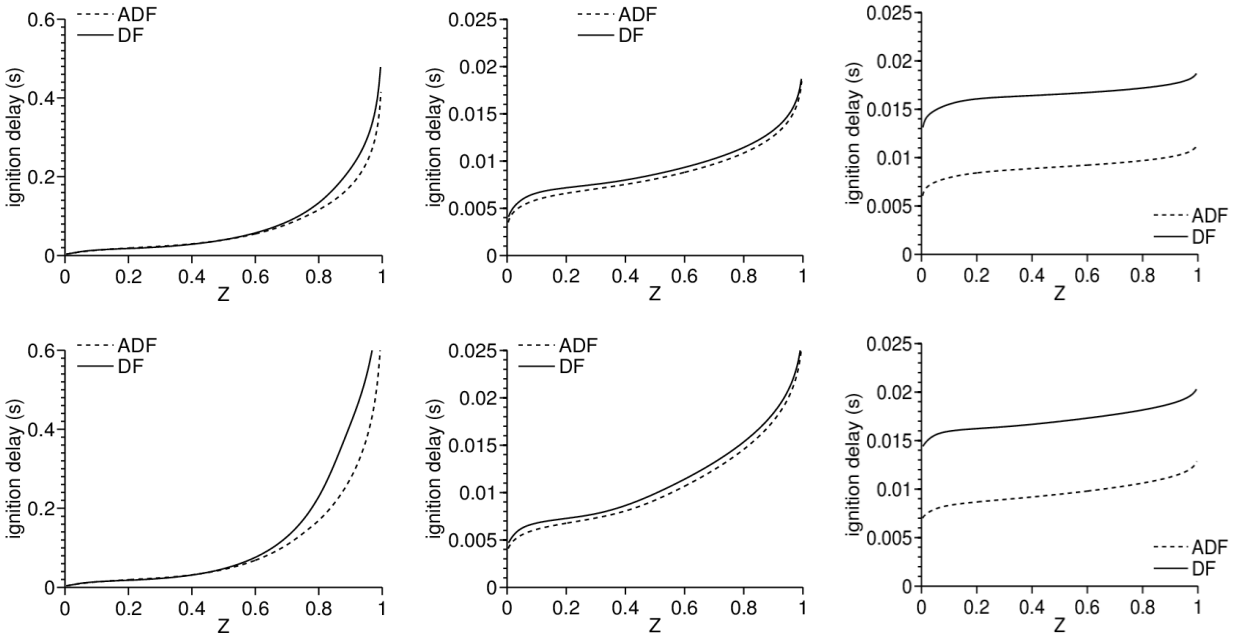

Figure 13. Ignition delay time for CH_4 until reaching c_F=0.05 (top) and c_F=0.3 (bottom) at strain rates a=1 (left), a=50 (center) and a=250 (right) 1/s.

Comparing the ADF model with the DF model, it is known that for long chain alkanes, such as C_7H_{16}, and high a values, the rich mixture fractions are more reactive with much shorter ignition delay times [13]. This does not occur in the other fuels that have been analyzed. Two facts that are interrelated seem to explain this artificial reactivity in the case of the C_7H_{16}:

- Due to the boundary and initial conditions (adiabatic curve) and the value of the stoichiometric mixture fraction, Z_{st}, which is very low for C_7H_{16} (0.062) while for H_2 has a high value (0.479), the combustion starts in the stoichiometric and slightly rich mixture fractions in the case of the C_7H_{16}. Unlike C_7H_{16}, for the H_2 and

CH_4 cases the first stages of ignition take place at very lean mixture fractions.

- The chemical source term for rich mixture fractions in the case of C_7H_{16} shows a very important increase at very low c values. This increase was shown in the color map of the chemical source term in Figure 7 and is the cause of the non-physical quenching point of the S-curve that was explained in the previous section. This behavior does not occur in the case of H_2 and CH_4 where the value of the chemical source term for rich mixture fractions is markedly low even for high c values.

The combination of these facts point out that the rich mixtures may act as artificial ignition kernels when low Y_c quantities are transported. Consequently, the ADF model does not have the ability to reproduce the combustion structure properly, especially at rich mixtures for the C_7H_{16}, if no correction is introduced. To moderate this behavior, a new limitation of the reactivity of the mixture, based on that suggested by Michel et al. [13], is imposed over the chemical source terms. For the definition of this limitation, first, a threshold value of c is chosen. In this work this value is fixed at $c^* = 5 * 10^{-4}$. Then, a time $t^*(Z)$ can be univocally defined as the time spent for each mixture fraction Z before reaching this c^* during the auto-ignition process of the HRs. The limitation is then defined as

$$\dot{\omega}_Y(Z,t) = \begin{cases} \left(\frac{t}{t^*(Z)}\right)^{\alpha} \dot{\omega}_Y{}^{FPI}(Z,c(t)) & if\ t < t^*(Z) \\ \dot{\omega}_Y{}^{FPI}(Z,c(t)) & if\ t \geq t^*(Z) \end{cases} \tag{12}$$

where t is the value of the current flamelet instant and α is a non-negative constant that has to be adjusted. Note that if $\alpha = 0$ no limitation is introduced and if $\alpha \to \infty$ the limitation becomes

$$\dot{\omega}_Y(Z,t) = \begin{cases} 0 & if\ t < t^*(Z) \\ \dot{\omega}_Y{}^{FPI}(Z,c(t)) & if\ t \geq t^*(Z) \end{cases} \tag{13}$$

For retaining the continuity of the chemical source term field and avoiding numerical perturbations it is recommended to assign a finite value to α. In this work the limitation is imposed over the whole range of mixture fractions values.

The proposed limitation is based on the Livengood and Wu approximation [34]. It is clear that $t^*(Z)$ can be conceived as an ignition delay for each mixture fraction. In this way, the reactivity related to each mixture is decreased or even cancelled during this ignition delay or, equivalently, while eq. (14), which expresses the

Livengood and Wu integral, is fulfilled.

$$\int_0^t \frac{dt}{\tau(Z,T(t),Y_k(t))} \leq 1 \tag{14}$$

In general, the ignition delay τ depends on the local conditions during the ignition process, that is, temperature (T) and mass fractions of the species (Y_k) for each mixture fraction. If it is supposed that the local conditions for a mixture fraction do not strongly change until its ignition during the flame combustion then a zero order approximation can be assumed. Therefore, τ only depends on the mixture fraction and the initial conditions (adiabatic curve) and, consequently, it can be defined as the time spent to reach a value of c^* during the HRs auto-ignition (that is $\tau(Z,T(0),Y_k(0)) = t^*(Z)$). Then, it follows that the limitation is applied while

$$\int_0^t \frac{dt}{\tau(Z,T(0),Y_k(0))} \leq 1 \quad \rightarrow \quad \frac{t}{t^*(Z)} \leq 1 \tag{15}$$

Eq. (15) is equivalent to the interval where the limitation is applied in eq. (12) and (13).

As was mentioned before, the potential function $\left(\left.t\right/_{t^*(Z)}\right)^{\alpha}$ that multiplies the chemical source term in eq. (12) is suggested as a way to avoid discontinuities in the chemical source term as for example may appear if eq. (13) is applied. In this way, since both the potential function and the chemical term $\dot{\omega}_Y{}^{FPI}(Z,c)$ are continuous (if a piecewise linear interpolation is used for $\dot{\omega}_Y{}^{FPI}$) their product is continuous too. Consequently, unphysical and numerical perturbations in the solutions of the ADF equation are eliminated with the application of this definition for the limitation. Additionally, parameter α provides a degree of freedom to adjust and optimize the behavior of the ADF solutions.

For n-heptane, the ADF model has been calculated with different values of the exponent α and the solutions have been compared with the DF solutions. The ignition delays are shown in Figure 14 and Figure 15 for $c_F = 0.05$ and $c_F = 0.3$, respectively.

As expected greater values of the exponent diminish the reactivity of the mixture fractions and, consequently, the ignition delay increases. Additionally, it is observed that when the strain rate becomes higher the effect of the limitation is more pronounced. Likewise, it becomes apparent that for high strain rates the limitation is needed even for lean and stoichiometric mixture fractions.

It is observed that with a value of $\alpha = 2$ excellent results are obtained when comparing the ADF solutions with the DF results, even for high strain rates close to a_{AI}, retrieving, consequently, the profile of the ignition delay provided by the DF model. Hence, $\alpha = 2$ is considered the most suitable value for parameter α.

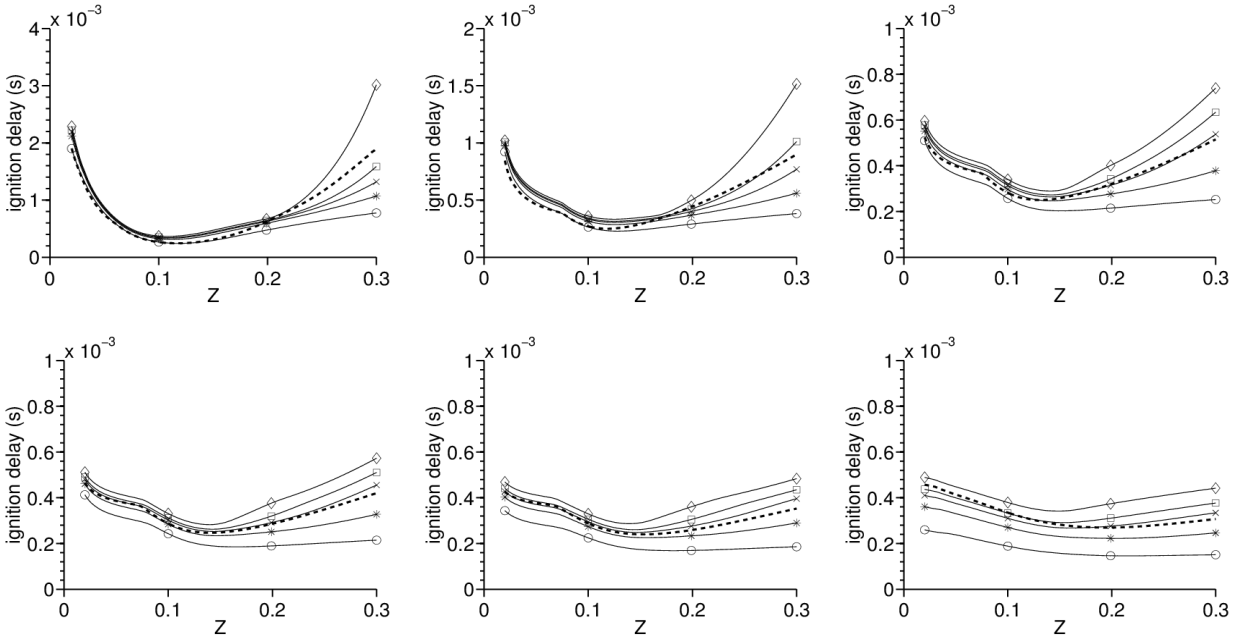

Figure 14. Ignition delay time for C_7H_{16} until reaching c_F=0.05 at strain rates a=1 (top left), a=10 (top center), a=50 (top right), a=100 (bottom left), a=200 (bottom center) and a=1000 (bottom right) 1/s. The dashed line corresponds to the DF solution. The solid lines correspond to the ADF solutions with the following legend: circles for no limitation, asterisks for α=1, crosses for α=2, squares for α=3 and diamonds for α=10.

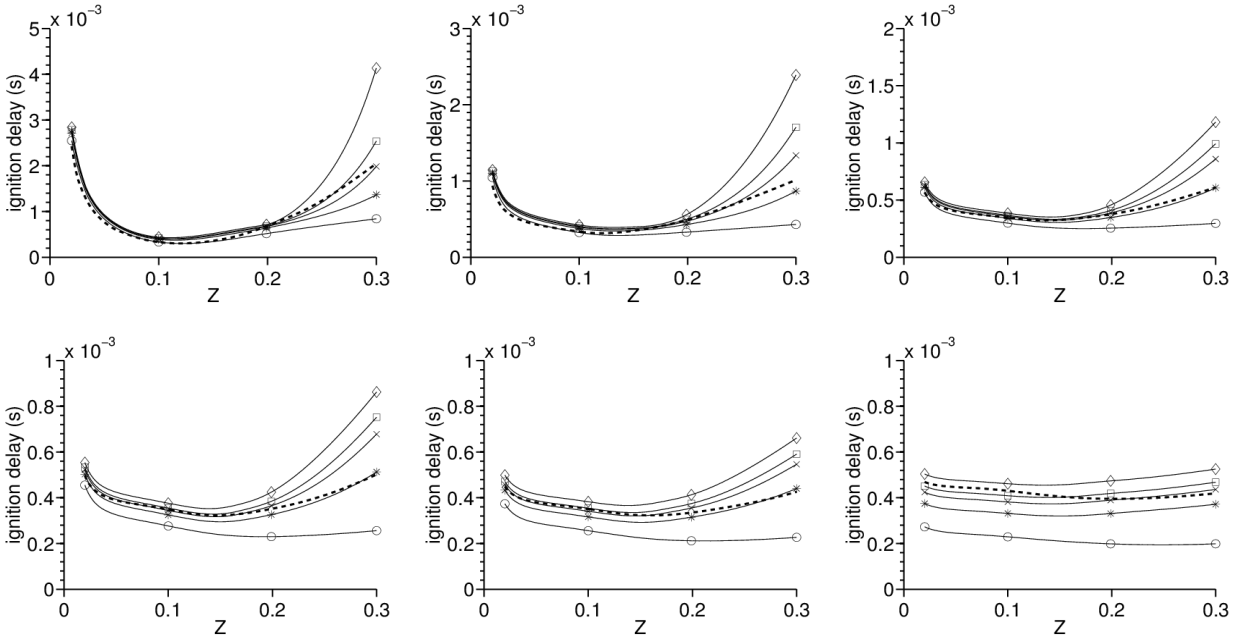

Figure 15. Ignition delay time for C_7H_{16} until reaching c_F=0.3 at strain rates a=1 (top left), a=10 (top center), a=50 (top right), a=100 (bottom left), a=200 (bottom center) and a=1000 (bottom right) 1/s. The dashed line corresponds to the DF solution. The solid lines correspond to the ADF

solutions with the following legend: circles for no limitation, asterisks for α=1, crosses for α=2, squares for α=3 and diamonds for α=10.

With the proposed limitation, results are considered satisfactory and it is observed that the ability of the ADF model to reproduce the ignition delay time has been significantly improved.

For analyzing the internal combustion structure, Figure 16 and Figure 17 show the transient profiles of Y_c for H_2 and CH_4, respectively. In both figures, the top plots correspond to flamelets in the auto-ignition range while the bottom plots correspond to flamelets in the ignition-extinction range. In this representation, the transient profiles correspond to the same value of the parameter $c2$ defined according to eq. (16).

$$c2(a,t) = \frac{\int_0^1 \left(Y_c(Z,a,t) - Y_{c,inert}(Z)\right) dZ}{\int_0^1 \left(Y_{c,steady}(Z,a) - Y_{c,inert}(Z)\right) dZ} \tag{16}$$

By definition, $c2$ ranges between 0 and 1 and, for a given flamelet, the correspondence from $c2$ to time is univocal. Variable $c2$ measures the global advancement of the whole flamelet. Note how the profiles defined by the same value of $c2$ between DF and ADF models do not necessarily match the same time instant. Hence, this comparison focuses on the analysis of the geometry of the (Z, Y_c) profile during the ignition propagation across the flamelet to check if the physics associated to this process is similarly reproduced by both models.

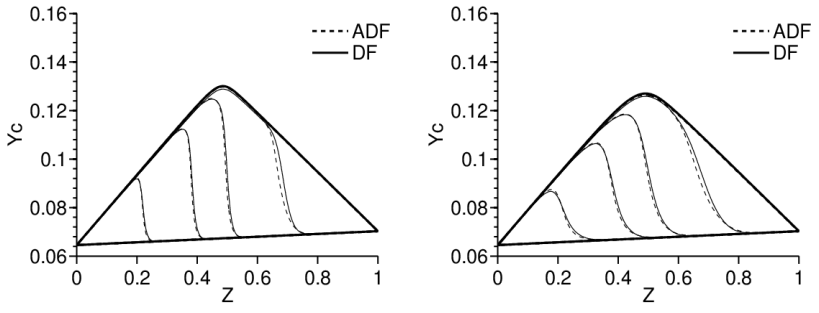

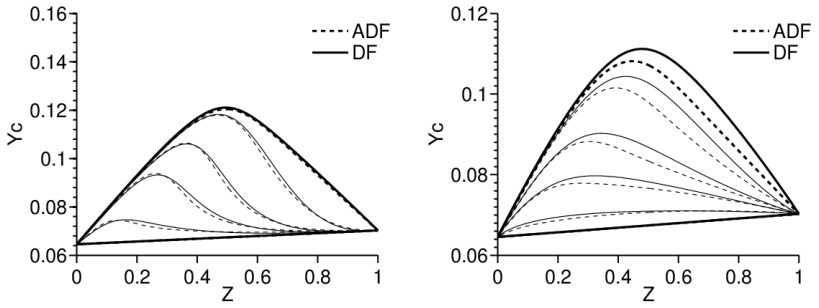

Figure 16. Profiles of (Z, Y_c) for H_2 and c2=0.1, 0.3, 0.5, 0.8 at strain rates a =10 (top left), a =100 (top right), a=1000 (bottom left) and a=5000 (bottom right) 1/s. Inert (c2=0) and steady-state (c2=1) solutions are included in bold.

As observed, DF and ADF models give very similar $(Z,\ Y_c)$ profiles for a given $c2$ value for both fuels. This confirms how, despite the additional simplifications introduced by the ADF model, the structure of the ignition propagation across the flamelet, traced by the morphology of the $(Z,\ Y_c)$ curve, is well-reproduced even for a values belonging to the ignition-extinction range as 1000 or 5000 1/s for H_2 and 800 or 2000 1/s for CH_4. Note how when a increases, the slope of the curves is softer due to the diffusion processes in Z-space and this phenomenon is also correctly reproduced by the ADF model. At high a values the differences between DF and ADF profiles in the figures are partially caused by the discrepancy between the steady-state regimes between both models and the fact that curves have been plotted at iso- $c2$ (see eq. (16)).

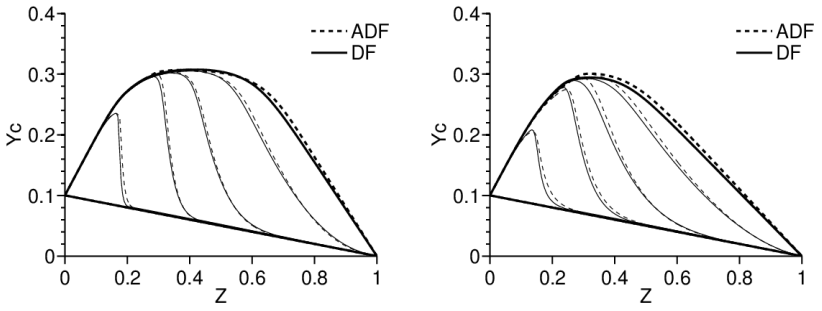

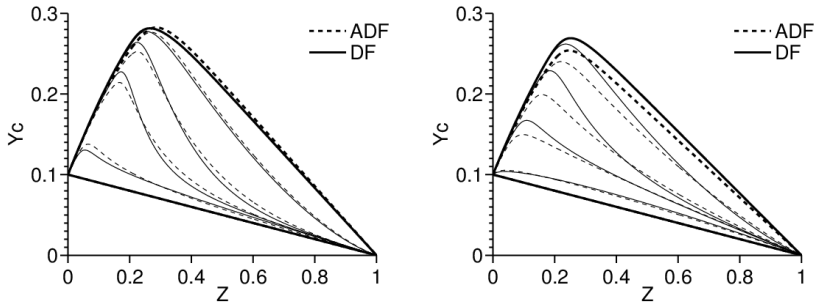

Figure 17. Profiles of (Z, Y_c) for CH_4 and c2=0.1, 0.3, 0.5, 0.8 at strain rates a=10 (top left), a=100 (top right), a=800 (bottom left) and a=2000 (bottom right) 1/s. Inert (c2=0) and steady-state (c2=1) solutions are included in bold.

Figure 18 shows the profiles $(Z,\ Y_c)$ for the fuel C_7H_{16} with the solutions given by the DF model and the ADF model defined with $\alpha = 2$. All the flamelets shown in the figure correspond to flamelets in the auto-ignition range. It is observed that the limitation avoids the chemical generation of progress variable at rich mixture fractions and so the profiles given by the ADF model are similar to those provided by the DF model. It is concluded that, in general terms, the DF solution can be accurately predicted with the ADF model if a limitation, as that proposed in this work, is imposed in the auto-ignition range.

Additionally, it is very interesting to compare the evolution of the $Y_{c,dot}$ variable ($\frac{\partial Y_c}{\partial t}$ in eq. (3)), which represents the temporal variation of Y_c including both mixing and chemical source terms. For that purpose, the contour plots for $Y_{c,dot}$ at given Z values and for the whole set of strain rates are represented in Figure 19 for H_2 and Figure 20 for CH_4. For each figure scales are common.

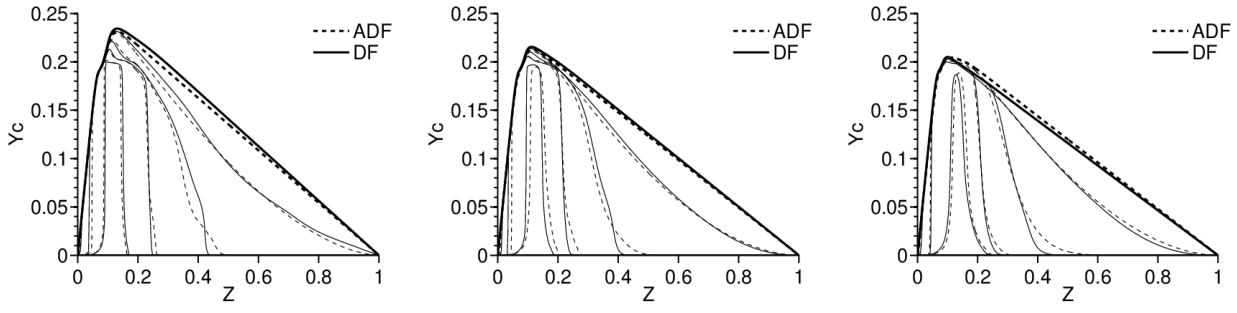

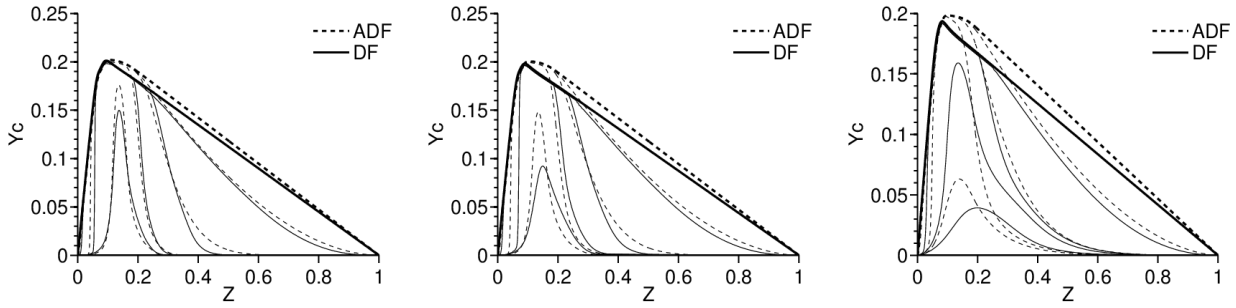

Figure 18. Profiles of (Z, Y_c) for C_7H_{16} and c2=0.1, 0.3, 0.5, 0.8 at strain rates a=1 (top left), a=10 (top center), a=50 (top right), a=100 (bottom left), a=200 (bottom center) and a=1000 (bottom right) 1/s. Inert (c2=0) and steady-state (c2=1) solutions are included in bold.

Both DF and ADF models correctly reproduce the physics since for lean mixture fractions maximum $Y_{c,dot}$ is observed for low a values. For these flamelets, the lean mixture fractions are especially reactive due to the boundary conditions in temperature, which implies that the combustion process starts in the lean mixture fraction range and it propagates later towards richer mixture fractions. When a is low the production of Y_c by the chemical source term is mainly used for increasing Y_c for that mixture fraction and a very low fraction of Y_c diffuses to the adjacent mixture fractions.

Nevertheless, when increasing a, the diffusion in Z-space promotes the transfer of higher fractions of the Y_c generated by the chemical source term to the surrounding mixture fractions. Consequently, $Y_{c,dot}$ decreases in the lean mixture fractions and increases in richer mixture fractions. Therefore, in these richer mixture fractions the maximum $Y_{c,dot}$ is observed for higher a values. This propagation of Y_c from lean to rich mixture fractions favors a more balanced advance of Y_c for all mixture fractions and avoids a profile with high gradients in the reactive zone for Y_c as observed in Figure 16 and Figure 17 for low a values.

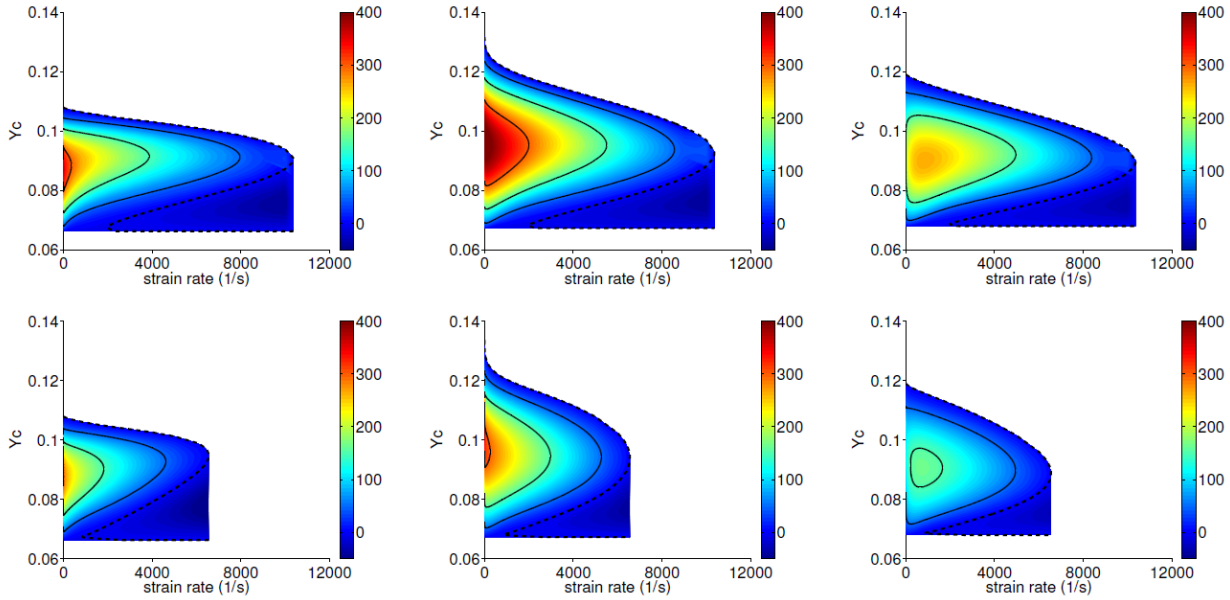

Figure 19. Contour plots of $Y_{c,dot}$ for H_2 using DF (top) and ADF (bottom) models, including lean (left), stoichiometric (center) and rich (right) mixture fractions. The dashed black lines represent the steady regime. The solid black lines correspond to $Y_{c,dot}$ isolines with values 50, 150 and 300 1/s.

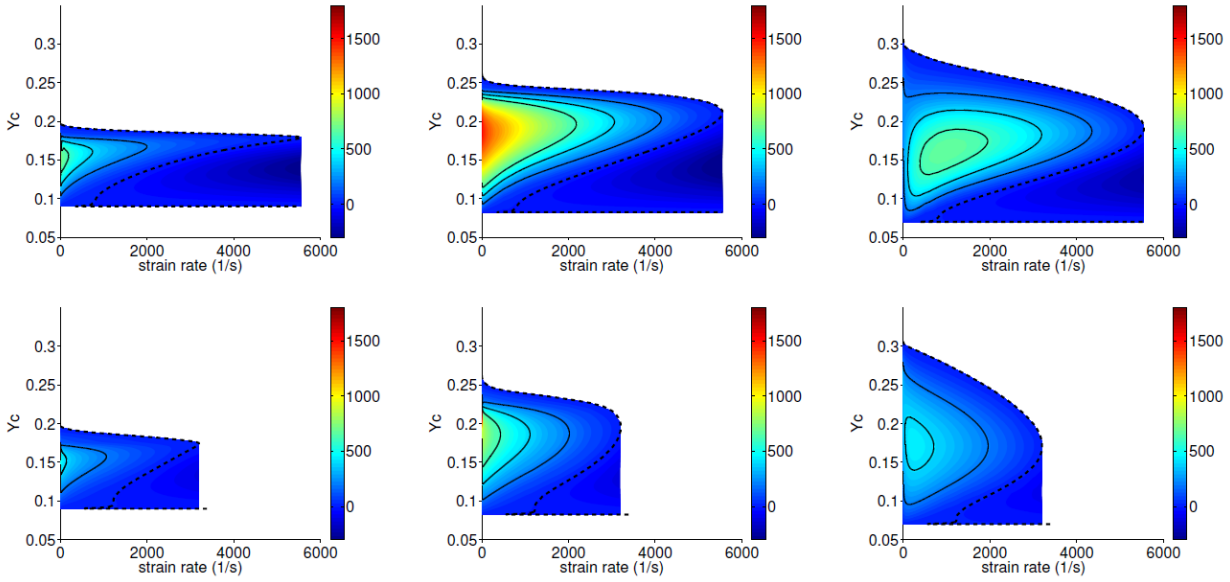

Figure 20. Contour plots of $Y_{c,dot}$ for CH_4 using DF (top) and ADF (bottom) models, including lean (left), stoichiometric (center) and rich (right) mixture fractions. The dashed black lines represent the steady regime. The solid black lines correspond to $Y_{c,dot}$ isolines with values 200, 400 and 600 1/s.

Effect of the progress variable definition

The influence of the Y_c definition in the results generated by the ADF model was already discussed in steady-state conditions, so here, the impact on the results in the unsteady regime is investigated following a similar approach. Thus, the results using the two Y_c definitions, PV1 and PV2, for CH_4 and C_7H_{16} flames are compared with the aim of determining the extent of the differences. In the C_7H_{16} case,

computations for both progress variable definitions have been carried out with a limitation defined in the whole range of mixture fractions and $\alpha = 2$.

Note how, as in the steady-state regime, the (Z, Y_c) profiles cannot be directly compared because they correspond to different Y_c definitions. To avoid this problem, a variable such as the temperature is used. The scope of this comparison is to show how the geometry of the (Z, T) profiles is affected by the definition of Y_c. Then, as in the DF-ADF models comparison, in this case, imposed values of $c2$, defined by eq. (16), are used instead of time and, therefore, the curves plotted in the following figures do not necessarily correspond to the same time instant.

Figure 21 contains the curves (Z, T) for CH_4 and Figure 22 for C_7H_{16}. For CH_4 the top plots correspond to flamelets in the auto-ignition range while the bottom plots correspond to flamelets in the ignition-extinction range. For C_7H_{16} all flamelets are located in the auto-ignition range since the shape of the S-curves on the ignition-extinction range is distorted, complicating the analysis of this range.

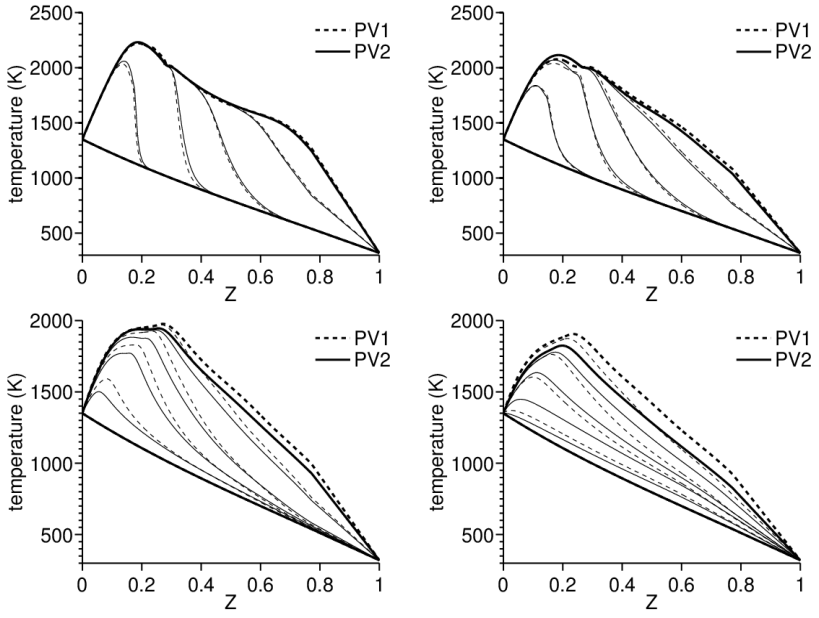

Figure 21. Profiles of (Z, T) for CH_4 using PV1 and PV2 and c2=0.1, 0.3, 0.5, 0.8 at strain rates a=10 (top left), a=100 (top right), a=800 (bottom left) and a=2500 (bottom right) 1/s. Inert (c2=0) and steady-state (c2=1) solutions are included in bold.

According to the figures, in the auto-ignition range the two Y_c definitions, PV1 and PV2, provide very similar profiles. Even in the ignition-extinction range (only shown for the case of the CH_4) the shape of the profiles is similar during the transient evolution. The differences between the curves shown in the figures are

mainly caused because the steady state is slightly different for the two progress variable definitions and these curves have been represented at iso-$c2$ values.

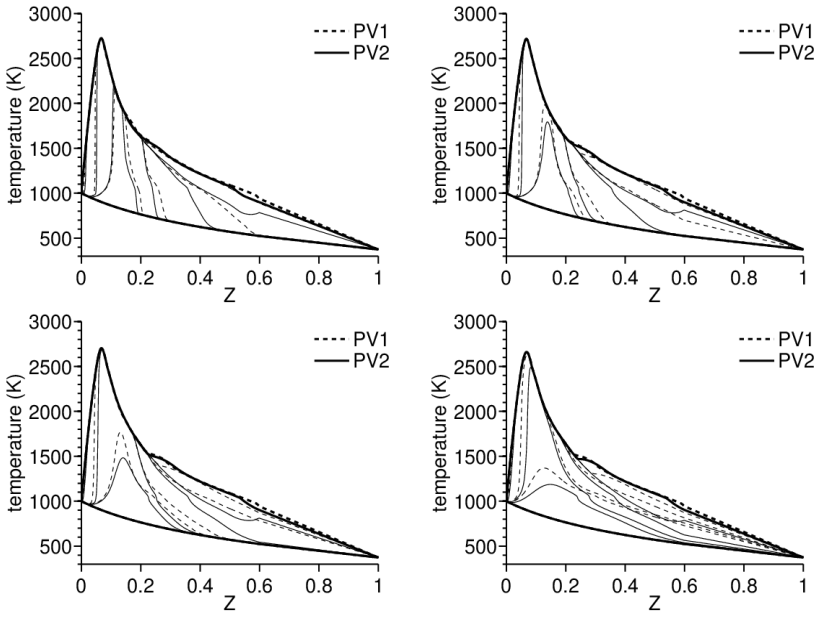

Figure 22. Profiles of (Z, T) for C_7H_{16} using PV1 and PV2 and c2=0.1, 0.3, 0.5, 0.8 at strain rates a=10 (top left), a=50 (top right), a=200 (bottom left) and a=1000 (bottom right) 1/s. Inert (c2=0) and steady-state (c2=1) solutions are included in bold.

Summarizing, solutions do not strongly depend on the selection of the progress variable definition, especially in the auto-ignition range and, in any case, differences are acceptable. This is expected since the differences between the two progress variable definitions increase as the strain rate becomes higher and when the strain rate equals to 0, no diffusion in Z-space, both progress variable definitions provide the same solution considering the ADF model assumptions.

5. Conclusions

The high computational cost of the DF model for solving flamelets for complex chemistry fuels encourages research to find additional simplifications. Among the different possibilities for tackling this problem, the ADF model is chosen because it allows a drastic reduction in the computational cost while managing complex chemical mechanisms. This computational time reduction is especially critical when flamelet models are applied to complex problems, such as the simulation of diesel engines, where boundary conditions span over wide intervals and, additionally, complex phenomena interact. Pollutant emissions modelling arise as one of these complex phenomena for which the use of complex chemistry in the calculations is mandatory and, consequently, it is necessary to use models that are able to manage

the corresponding chemical mechanisms.

The two main hypotheses of this model consist of solving the transport species equation only for one variable, denoted as the progress variable, and assuming that the progress variable chemical source term does not depend on the diffusion in Z-space. The validity of these hypotheses is analyzed by the direct comparison of this simplified ADF model with the DF model.

In the steady-state regime the auto-ignition range is in general terms well-reproduced by the ADF model independently of the fuel characteristics, but noticeable divergences were detected in the ignition-extinction range which increase with the fuel chemical complexity. For all the fuels investigated it was observed how the quenching point has a greater strain rate value for the DF model than for the ADF model.

Additionally, the definition of the progress variable has no marked effect on the ADF solutions in the auto-ignition range.

For computing the ADF unsteady solutions from the HRs database, the chemical source terms corresponding to low progress variable values have to be carefully calculated. Additionally, it is important to define the chemical source term with a continuous function for avoiding numerical perturbations. In order to fulfill these requirements, a method is proposed in the present paper.

Comparing DF and ADF models in the unsteady regime, it can be concluded that the ignition delay time is well-reproduced. For the C_7H_{16} fuel, excellent ignition delay results can be achieved, even for high strain rates, if the newly developed limitation in the chemical source term is imposed. Likewise, for all the fuels the ignition propagation across the flamelet is well described by the ADF model even for high strain rates. Therefore, it has been shown how the ignition propagation across the flamelet does not strongly depend on the assumptions taken in the ADF model.

In the unsteady regime, the progress variable definition has low impact on the ignition propagation across the flamelet and then, results are independent (with acceptable differences) of the progress variable definition.

For concluding the research, although non-negligible deviations appear when the ADF hypotheses are applied to the ignition-extinction range, the ADF model enables the auto-ignition range to be properly modeled with acceptable

discrepancies in comparison with the DF model with a very low computational cost.

Thus, the ADF model should be considered for CFD modeling when the turbulent combustion is mainly dominated by auto-ignition processes and ignition-extinction phenomena are not relevant. This mainly depends on the fuel chemical properties and the boundary conditions imposed by the flow and in a great variety of industrial devices correspond to the usual thermo-fluid dynamics work conditions. Important examples of these devices are diesel engines and diesel-like sprays, which match these conditions and, then, the ADF model is suitable for their simulation.

Acknowledgments

Authors acknowledge that this work was possible thanks to the *Ayuda para la Formación de Profesorado Universitario* (FPU 14/03278) belonging to the *Subprogramas de Formación y de Movilidad del Ministerio de Educación, Cultura y Deporte* from Spain. In addition, this study was partially funded by the *Ministerio de Economía y Competitividad* from Spain in the frame of the COMEFF (TRA2014-59483-R) national project.

Likewise, authors would like to express their acknowledgment to Dr. Bertrand Naud for providing LFLAM code used for solving the DF model equations.

References

[1] T. Poinsot, D. Veynante, Theoretical and numerical combustion, Edwards, 2005.

[2] N. Peters, Turbulent combustion, Cambridge University Press, 2000.

[3] A.C. Benim, K.J. Syed, Laminar flamelet modelling of turbulent premixed combustion, Appl. Math. Modelling 22 (1998) 113-136.

[4] E. Mastorakos, Ignition of turbulent non-premixed flames, Prog. Energy Combust. Sci. 35 (2009) 57-97.

[5] N. Peters, Laminar diffusion flamelet models in non-premixed turbulent combustion, Prog. Energy Combust. Sci. 10 (1984) 319-339.

[6] H. Pitsch, M. Chen, N. Peters, Unsteady flamelet modeling of turbulent hydrogen-air diffusion flames, Symposium (International) on Combustion 27 (1998) 1057-1064.

[7] G. D'Errico, T. Lucchini, F. Contino, M. Jangi, X.S. Bai, Comparison of well-mixed and multiple representative interactive flamelet approaches for diesel spray combustion modelling, Combust. Theor. Model. 18 (2014) 65-88.

[8] H. Barths, C. Hasse, N. Peters, CFD modeling of non-premixed combustion in DI diesel engines. Int. J. Engine Res. 1 (2000) 249–267.

[9] H. Barths, C. Hasse, G. Bikas, N. Peters, Simulation of combustion in DI diesel engines using an eulerian particle flamelet model, Proc. Combust. Inst. 28 (2000) 1161–1168.

[10] P.K. Jha, C.P. Groth, Tabulated chemistry approaches for laminar flames: evaluation of flame-prolongation of ILDM and flamelet methods, Combust. Theor. Model. 16 (2012) 31-57.

[11] O. Gicquel, N. Darabiha, D. Thevenin, Laminar premixed hydrogen/air counterflow flame simulations using flame prolongation of ILDM with differential diffusion. Proc. Combust. Inst. 28 (2000) 1901-1908.

[12] J.A. Van Oijen, L.P.H. de Goey, Modelling of premixed laminar flames using flamelet-generated manifolds, Combust. Sci. Technol. 161 (2000) 113-137.

[13] J.B. Michel, O. Colin, D. Veynante, Modeling ignition and chemical structure of partially premixed turbulent flames using tabulated chemistry, Combust. Flame 152 (2008) 80-99.

[14] J.B. Michel, O. Colin, C. Angelberger, D. Veynante, Using the tabulated diffusion flamelet model ADF-PCM to simulate a lifted methane-air jet flame, Combust. Flame 156 (2009) 1318-1331.

[15] J. Tillou, J.B. Michel, C. Angelberger, D. Veynante, Assessing LES models based on tabulated chemistry for the simulation of Diesel spray combustion, Combust. Flame, 161 (2014) 525-540.

[16] J.M. Desantes, J.M. García-Oliver, R. Novella, E.J. Pérez-Sánchez, Application of an unsteady flamelet model in a RANS framework for spray A simulation, Appl. Therm. Eng. 117 (2017) 50-64.

[17] J.B. Michel, O. Colin, A tabulated diffusion flame model applied to diesel engine simulations, J. of Engine Research 15 (2014) 346–369.

[18] O. Colin, J.B. Michel, A two-dimensional tabulated flamelet combustion model for furnace applications, Flow Turbul. Combust. (2016) 1–32.

[19] H. Pitsch, N. Peters, A consistent flamelet formulation for nonpremixed combustion considering differential diffusion effects, Combust. Flame 114 (1998) 26–40.

[20] M.D. Emami, A.E. Fard, Laminar flamelet modeling of a turbulent CH4/H2/N2 jet diffusion flame using artificial neural networks, Appl. Math. Modelling 36 (2012) 2082-2093.

[21] D.A. Lysenko, I.S. Ertesvåg, K.E. Rian, Numerical simulation of non-premixed turbulent combustion using the eddy dissipation concept and comparing with the steady laminar flamelet model, Flow Turbul. Combust. 93 (2014) 577–605.

[22] C.D. Pierce, P. Moin, Progress-variable approach for large-eddy simulation of non-premixed

turbulent combustion, J. Fluid Mech. 504 (2004) 73–97.

[23] L.R. Petzold, Sandia National Laboratories Report, SAND82-8637, 1982.

[24] B. Naud, R. Novella, J.M. Pastor, J.F. Winklinger, RANS modelling of a lifted H2/N2 flame using an unsteady flamelet progress variable approach with presumed PDF, Combust. Flame 162 (2015) 893-906.

[25] CHEMKIN-PRO, Reaction Design, San Diego, 2008.

[26] R. Cabra, T. Myhrvold, J.Y. Chen, R.W. Dibble, A.N. Karpetis, R.S. Barlow, Simultaneous laser Raman-Rayleigh-LIF measurements and numerical modeling results of a lifted turbulent H2/N2 jet flame in a vitiated coflow, Proc. Combust. Inst. 29 (2002) 1881-1888.

[27] R. Cabra, J.Y. Chen, R.W. Dibble, A.N. Karpetis, R.S. Barlow, Lifted methane-air jet flames in a vitiated coflow, Combust. Flame 143 (2005) 491-506.

[28] L. Pickett, G. Bruneaux, R. Payri, Engine combustion network, Sandia National Laboratories, Livermore, CA, http://www.ca.sandia.gov/ecn, 2016.

[29] P. Saxena, F.A. Williams, Testing a small detailed chemical-kinetic mechanism for the combustion of hydrogen and carbon monoxide, Combust. Flame 145 (2006) 316-323.

[30] G. Smith, D.M. Golden, M. Frenklach, N.W. Moriarty, B. Eiteneer, M. Goldenberg, C.T. Bowman, R.K. Hanson, S. Song, C. William, J. Gardiner, V.V. Lissianski, Z. Qin, GRI-mech web site http://www.me.berkeley.edu/gri-mech/, 1999.

[31] T. Zeuch, G. Moreac, S.S. Ahmed, F. Mauss, A comprehensive skeletal mechanism for the oxidation of n-heptane generated by chemistry-guided reduction, Combust. Flame 155 (2008) 651-674.

[32] C. Pera, O. Colin, S. Jay, Development of a FPI detailed chemistry tabulation methodology for internal combustion engines, Oil Gas Sci. Technol. 64 (2009) 243-258.

[33] J. Tillou, Développement d'une modélisation basée sur la tabulation de schémas cinétique complexe pour la simulation aux grandes échelles (LES) de l'autoflammation et de la combustion turbulente non prémélangée dans les moteurs à pistons. Ph. D. Thesis, École Centrale Paris, 2013.

[34] J.C. Livengood, P.C. Wu, Correlation of autoignition phenomena in internal combustion engines and rapid compression machines, Symposium (Int.) on Combustion 5 (1955) 347-356.